Alkenone-based Evidence of Holocene Slopewater Cooling in the Northwest Atlantic

by

Jessie M. Kneeland
B.S. Geology
California Institute of Technology, 2004

Submitted to the Department of Earth, Atmospheric, and Planetary Sciences

in partial fulfillment of the requirements for the degree of

Master of Science in Climate Physics and Chemistry

at the

MASSACHUSETTS INSTITUTE OF TECHNOLOGY

September 2006

Author .....
Department of Earth, Atmospheric, and Planetary Sciences
August 11, 2006

Certified by .....
Julian P. Sachs
Associate Professor
Thesis Supervisor

Accepted by .....
Maria T. Zuber
E.A. Griswold Professor of Geophysics
Head, Department of Earth, Atmospheric and Planetary Sciences

Alkenone-based Evidence of Holocene Slopewater Cooling in the Northwest Atlantic

by

Jessie M. Kneeland

B.S. Geology

California Institute of Technology, 2004

Submitted to the Department of Earth, Atmospheric, and Planetary Sciences
on August 11, 2006, in partial fulfillment of the
requirements for the degree of
Master of Science in Climate Physics and Chemistry

Abstract

Alkenone-based estimates of sea surface temperature (SST) in the northwest Atlantic during the last 10,000 years are presented and used to assess scenarios for Holocene climate variability. Alkenone concentration and unsaturation records are presented from cores KNR140-39GGC, KNR140-51GGC, MD95-2028, MD95-2031, and MD95-2025 from the Blake Ridge (32°N), Carolina Slope (33°N), Fogo Seamount (42°N), Narwhal (44°N), and Orphan Basin (50°N) respectively. The southernmost core, from the Blake Ridge, indicates very little temperature variation over the Holocene. Somewhat inshore and to the north of that location, the Carolina Slope record shows a slight cooling trend of about 1.5°C over the past 5,000 years, which is interrupted by a brief but sudden drop of about 1°C between 3,000 and 2,000 years before present. Lack of age control for the core from Fogo Seamount prevents any conclusions about the time frame of alkenone variation at that location. At the Narwhal site, which is not far from the Laurentian fan, a strong and consistent cooling of 9°C is the most recent pattern of variation. Alkenone concentrations from the Orphan Basin were not sufficient for reliable measurement of a Holocene temperature trend. The general pattern of strong cooling in the northern slope water region and very modest cooling south of Cape Hatteras, where the Gulf Stream separates from the coastline and heads out to sea, may suggest a shift in mean Gulf Stream path as a possible culprit for the temperature record seen at the Narwhal site. However, changes of incoming solar radiation or seasonality of alkenone production over the Holocene provide alternative mechanisms for alkenone temperature variation.

Thesis Supervisor: Julian P. Sachs
Title: Associate Professor

Acknowledgments

I wish to thank my advisors, Julian Sachs and Carl Wunsch, for the guidance and knowledge they provided while I prepared for and completed this thesis. Carl encouraged me to take a critical look at the usual assumptions made in paleoceanography, and to be scientifically rigorous in my thinking. Julian provided an abundance of enthusiasm and plenty of ideas and access to samples to keep me busy.

I am very grateful to Carl for securing funding for my studies and work on this project; NASA is thanked for this support. Additional financial support was from a Robert R Shrock Graduate Fellowship, and I am thankful to Vicki McKenna for securing this support that allowed me to complete my thesis.

Lloyd Keigwin at WHOI is gratefully acknowledged for allowing me to sample cores he collected and for providing fruitful discussions and information about data interpretations. Ellen Roosen and Jim Broda helped me collect samples at WHOI. John King at URI provided access to sediment cores and sampling space in his lab, and his students were very helpful as well.

Several Sachs Lab members provided a good deal of laboratory assistance, for which I am grateful. Rienk Smittenberg and Zhaohui Zhang advised me on laboratory equipment and techniques. Monica Byrne provided inspiration and encouragement. Katharina Pahnke helped me to learn to measure alkenones, and she sampled sediment cores with me.

Finally, I'd like to thank my family and friends for providing the supportive environment that helped me get to MIT in the first place and then complete this thesis. My parents always encouraged me to set my goals high and persevere in my work, and I'm thankful that they also reminded me to have enough fun to stay sane. Above all, I am most grateful to Marcus, without whom I would have missed dinner more than I'd like to admit.

Contents

List of Figures

List of Tables

Chapter 1

Introduction

In the context of a 65 million year record of global climate fluctuations [53], the current interglacial period, known as the Holocene, is thought to be a period of fairly stable climate [15]. With the exception of an abrupt transition to colder temperatures at around 8200 years before present (B.P.) [2], Holocene temperatures reconstructed from oxygen isotopes in Greenland ice cores appear to have remained almost constant, in contrast to the glacial-interglacial cycles of the previous 250,000 years [10].

Recent studies of sea surface temperatures in the northwest Atlantic based on alkenone unsaturation ratios have indicated that ocean temperatures decreased by about 10°C over the Holocene [21]. This result is surprising, and seemingly at odds with the previous understanding of Holocene temperatures [10]. Though there has been some previous alkenone evidence of a modest cooling of 1 - 3°C, those data apparently conflicted with oxygen isotope and species abundance data from planktonic foraminifera from the same sites that showed no cooling trend [27].

The monotonic decrease in sea surface temperature seen in alkenone data from the Laurentian Fan is not undisputed by evidence from foraminiferal oxygen isotopes [21], and a clear climatic mechanism for such a cooling is not obvious. These uncertainties in the interpretation of Laurentian Fan alkenone data prompted a need for additional data.

In order to examine the timing and extent of the apparent surface ocean cooling over the Holocene, we selected several sites in the slope water region of the north-

western Atlantic for further alkenone-based analysis. The alkenone technique relies on measuring the relative proportions of several specific unsaturated methyl ketones, compounds produced in the mixed layer of the ocean by coccolithophorids, a type of phytoplankton. The alkenone unsaturation parameter $U_{37}^{k'}$ has been previously established as a proxy for mean annual sea surface temperature in numerous studies [37, 39, 46, 29].

This thesis begins with a review of the alkenone unsaturation parameter $U_{37}^{k'}$ and its use as a proxy for sea surface temperature. A review of current understanding of Holocene climate follows. A section describing the oceanography and climate of the slope water region places the study sites in a geographic and climatic context. Sections describing analytical methods used and results obtained in this study follow the review sections. We conclude with discussion of possible explanations for the apparent Holocene cooling in slope waters substantiated by the alkenone data presented here.

Chapter 2

Background: Holocene climate and oceanography of the North Atlantic and Alkenone Paleothermometry

2.1 Holocene Climate of the North Atlantic

2.1.1 Proxy records

Many paleoceanographic proxies have been used to decipher the history of climate during the Holocene, or roughly the last 10,000 years. An early indication from the $\delta^{18}O$ in Greenland ice seemed to indicate that climate, or more specifically air temperature over Greenland, had been quite stable over the Holocene, particularly compared to the magnitude of variability during glacial periods [15, 10].

The only apparent Holocene climate fluctuation of any significance in Greenland is the 8.2 kyr cold event [2]. At this time, methane concentration, accumulation rate, and δ^{18}O of the ice all decreased and salt concentrations in the ice increased. These changes indicate a drier and dustier period approximately 5°C colder over Greenland that lasted several hundred years [2]. Evidence from the slope water region

in the western north Atlantic indicate that ocean temperatures there may have been suppressed around that time for as long as 700 years [21]. Although the effects of this event on atmosphere and ocean temperatures seem prolonged, the cause is now thought to have been a quick release of about 5 Sv (1 Sv = 10^6 m^3/s) of flood water from glacial Lake Agassiz lasting less than a year [7] .

The high resolution record of CO_2 in ice from Siple Dome, Antarctica, demonstrates that CO_2, an important "greenhouse gas", was not constant over the Holocene [1]. The compilation by Ahn and coworkers [1] of that CO_2 data with other previously published data from various Antarctic ice cores provides a good picture of how several important climate variables covaried, and that figure is reproduced as Figure 2-1 here.

Evidence for sea surface temperature variations comes from many locations in the north Atlantic area. Hald et al. [16] report foraminiferal assemblage data that indicate that slope SSTs in the Norwegian Sea near Svalbard increased during the earliest Holocene (approximately 10,800 cal. years BP according to radiocarbon dating) by about 3 - 4°C, remained at that higher temperature until about 8800 cal. years BP, and then decreased again.

Marchal and coworkers [27] provided a statistically rigorous examination of ocean temperature evidence from multiple proxies. They found that alkenone-based sea surface temperature records from seven locations around the northeast Atlantic and Mediterranean all show a statistically significant cooling over the Holocene. However, that result stood in sharp contrast to evidence they examined from foraminiferal $\delta^{18}O$ and foraminiferal abundance data, which show no clear temperature trend. Diatom assemblages from several of their cores indicate a possible cooling of up to 5°C over the period, but neither the timing nor magnitude of the diatom reconstruction agrees with the alkenone evidence, where they occur in the same core. Though the statistical tests of Marchal and coworkers [27] demonstrate the fidelity of trends in the alkenone data, they also demonstrate the significance of a lack of trend in the foraminifera data.

Another compilation of alkenone-based SST records by Lorenz and coworkers [26] also found a general pattern of surface cooling over the middle and late Holocene in

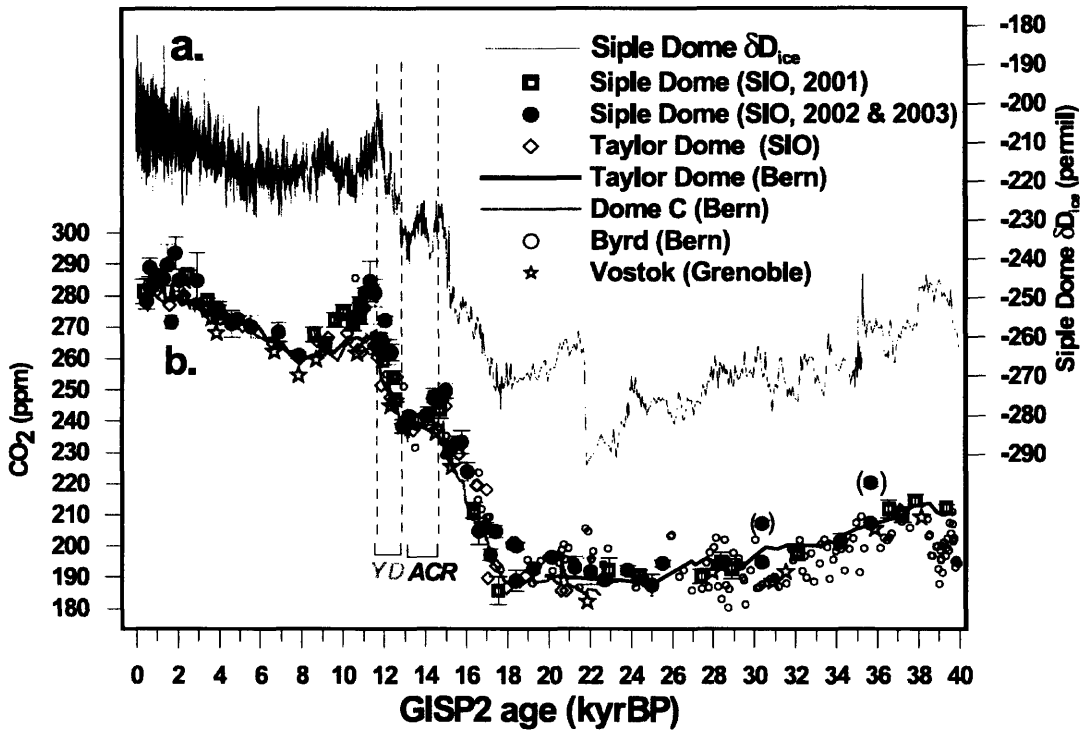

Figure 2-1: CO_2 concentration in Antarctic ice on the GISP2 age scale, from Ahn et al., 2004 [1].

the extratropics.

2.1.2 Modeling studies

Several models of Holocene climate have also indicated significant variation in ocean temperature over this period.

Renssen et al. [41] employed a coupled model including atmosphere, ocean, sea ice, and vegetation to simulate variation in atmosphere and ocean circulation and changes in sea surface temperature during the Holocene. The model included realistic insolation and prescribed methane and carbon dioxide concentrations estimated from Raynaud et al. [40]. The modeled temperature decrease in high northern latitudes of 2^oC over the Holocene is broadly consistent with proxy data.

Lorenz and coworkers [26] explored temperature trends over the past 7000 years in order to understand the alkenone temperature data they had compiled. Their model results indicated a mean warming of the northwest Atlantic near the Grand Banks of approximately 1°C, and no clear trend in the slope water south of that region. However, they calculated a decrease in summer temperature and increase in winter temperature in the same area that is consistent with the lower insolation contrast between summer and winter at Northern mid-latitudes in the early Holocene.

2.2 Oceanographic setting and climatology of the slope water region

2.2.1 Surface currents

The dominant oceanographic feature in the surface northwest Atlantic is the Gulf Stream. Warm waters of the Caribbean Current pass through the Florida Straits, join up with the Antilles Current, and then continue up the coast of the U.S. as the Gulf Stream, closely following the edge of the continental shelf. The Gulf Stream then separates from the coast by Cape Hatteras and heads out into the open ocean. From that point, the path of the Gulf Stream is highly variable, and a considerable

number of Gulf Stream meanders separate off into eddies known as "cold core rings" and "warm core rings" if they move south or north from the Stream, respectively. A coordinated survey in 1950 employed several U.S. Navy and research vessels to observe the Gulf Stream in a coordinated way, and one key result was confirmation that the eddies form when large amplitude meanders in the Gulf Stream close off [14]. A statistical study of satellite observations found that at least 24% of Gulf Stream crests (meanders to the north of the mean path) separate off to form warm core rings. These warm core rings are particularly important to the slope water region between the Gulf Stream and the continental shelf, because the eddies transport anomalously warm and salty water northward.

In addition to mesoscale eddies coming off of the Gulf Stream, the slope water is influenced by additional currents, particularly the Labrador Current and a so-called "slopewater current [14]." The slopewater current flows eastward through the slope water region after splitting off from the Gulf Stream [33], and the Labrador Current flows south and westward from the Labrador Sea and loops around the Grand Banks. The Labrador Current cools and freshens the northwest Atlantic slope waters. A map illustrating the surface currents in the slope water region is shown in Figure 2-2, from Pickart et al., 1999 [33].

2.2.2 The Gulf Stream separation

From the first attempts to write down a set of governing equations (e.g. Munk, 1950 [30]) to more recent and more complicated modelling efforts, many oceanographers have sought to understand what controls the mean circulation and variability in the northern Atlantic Ocean. Even a simple model of a rectangular basin where the Coriolis parameter varies with latitude is sufficient to explain the need for western-intensification of the overall surface gyre circulation in the northern Atlantic [47].

However, models and modellers still disagree over what controls the separation of the Gulf Stream from the coast at Cape Hatteras. Indeed, many models are unable to simulate the observed separation of the Gulf Stream, even in the presence of realistic bottom topography. Numerous hypotheses about the mechanism of Gulf Stream

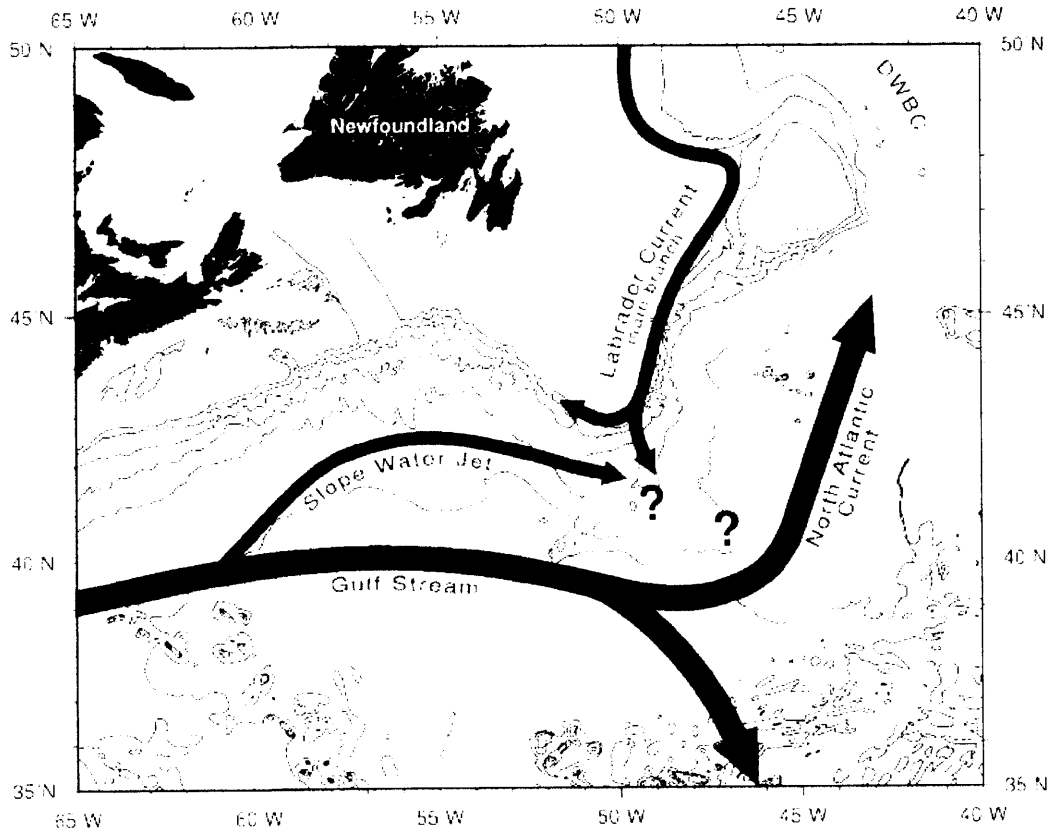

Figure 2-2: Surface currents in the slope water region. Contours show 200 m, 1000 m, 2000 m, 3000 m, 4000 m, and 5000 m depth. Reproduced from Pickart et al., 1999 [33].

separation are still being debated. One of the first hypotheses proposed was that the western boundary current separates from the coast at the latitude of zero wind curl [30]. Another prominent idea is that separation is due to interaction between the surface Gulf Stream and the Deep Western Boundary Current [50]. Another possibility, that separation is controlled by the joint effect of baroclinicity and relief (JEBAR), relies on contribution of density stratification and non-negligible bottom topography to the overall vorticity budget to explain the seaward bend in the Gulf Stream's path (see e.g. Myers et al., 1996 [31]). The mechanism of Gulf Stream separation is an outstanding problem in physical oceanography, and the possibility that the separation point may have differed under different climatological conditions bears further exploration.

2.2.3 The slope water

A compilation of hydrographic data from the slope water region revealed some significant patterns of circulation and variability [33]. As Fuglister and Worthington [14] initially identified, the slopewater current is observed as a jet unique from the Gulf Stream. Using an empirical orthogonal function (EOF) analysis of a series of hydrographic sections at either 50 or 55°W, Pickart et al. [33] found that in the slope water region, the slopewater jet and Labrador Current either strengthen or weaken in concert. In their strengthened state, the slopewater jet moves onshore. The deep circulation in these sites seems to covary with the surface flows as well. During times of strengthened surface currents, the flow at greatest depth, the southward-flowing Denmark Strait Overflow Water, is also strengthened relative to its mean. In contrast, the mid-level flow of the Labrador Sea Water is weakened.

A recent study by Dupont et al. [12] analyzed the heat, volume and salt budgets in the slope water region using results from a high-resolution ocean circulation model. Their primary conclusion is that properties in the slope water area are set by influences from the Gulf Stream, Slope Water Current, and Labrador Current, and by fluxes of heat from sea surface to atmosphere. They implied that under a slightly warmer climate, the formation of Slope Water would be decreased and the region would be

more strongly influenced by Gulf Stream properties.

2.2.4 Climatology: the North Atlantic Oscilation

The dominant climatological feature in the North Atlantic on interannual to decadal time-scales is the North Atlantic Oscillation (NAO). Similar to the better-known El Niño - Southern Oscillation (ENSO), the NAO is a coupled oscillation in the ocean and atmosphere. In the positive phase of the NAO, atmospheric pressure is higher over the Azores and lower over Iceland, compared to the mean. A positive NAO index is correlated with slightly increased sea surface temperature in the slope water region [28].

2.3 Alkenone unsaturation ratio as a sea surface temperature proxy

The use of alkenone unsaturation ratios as a proxy for sea surface temperature (SST) has recently gained broad application in the paleoceanography field. Volkman et al. [52] first reported the existence of the C_{37} - C_{39} methyl and ethyl ketones with two or three double bonds that later became commonly referred to as "alkenones." An initial study by Brassell et al. [6] showed that the degree of unsaturation in long-chain ketones produced by certain coccolithophorids was related to growth temperature. Since then, many workers have cultured the haptophyte algae which produce unsaturated C_{37} alkenones to establish the specific temperature (e.g. [37, 39]) nutrient [51, 38], and light [51, 38] dependence of the unsaturation patterns.

Core-top calibration studies [39, 45, 42, 29] have compared the alkenone unsaturation ratios of material extracted from sediments to the seasonal and annual sea surface temperature of overlying waters. Studies of alkenones extracted from near-surface seawater offer snapshots of water-column alkenone inventories that are difficult to compare with core-top studies, which examine alkenones produced over a much longer time period. Nonetheless, studies of alkenones in seawater particulate

organic matter provide additional information about the total amount and relative proportions of different alkenone compounds produced under a range of ocean conditions [4, 36, 34]. When comparing alkenone studies, it is important to differentiate between the source of the measured alkenones (e.g. core-top sediments, algal culture, or seawater) and the parameters to which they are being compared (e.g. seasonal or annual average sea surface temperature, culture growth temperature, or instantaneous sea surface temperature.)

2.3.1 Calibration of $U_{37}^{k'}$ as a temperature proxy

The first calibration between alkenone unsaturation ratios and temperature came from Brassell et al. [6], who introduced the use of the U_{37}^{k} index, which is defined as

$$U_{37}^{k} = \frac{[C_{37:2}] - [C_{37:4}]}{[C_{37:2}] + [C_{37:3}] + [C_{37:4}]} \tag{2.1}$$

where $[C_{37:2}]$, $[C_{37:3}]$, and $[C_{37:4}]$ represent concentrations of di-, tri-, and tetra-unsaturated C_{37} methyl ketones respectively. These three compounds, whose structures are shown in Figure 2-3, have been identified as (E,E)-15,22-heptatriacontadien-2-one, (E,E,E)-8,15,22-heptatriacontatrien-2-one, and (E,E,E,E)-8,15,22,29-heptatriatetraen-2-one by several groups [11, 52].

Prahl and Wakeham [37] first introduced the use of $U_{37}^{k'}$, which differs from the U_{37}^{k} index only in the neglect of the tetra-unsaturated C_{37} methyl ketone. Specifically, the $U_{37}^{k'}$ index is defined as

$$U_{37}^{k'} = \frac{C_{37:2}}{C_{37:2} + C_{37:3}} \tag{2.2}$$

One commonly-used calibration between $U_{37}^{k'}$ comes from a core-top study by Müller et al. [29]. By comparing core-top values of $U_{37}^{k'}$ from over a hundred samples with mean annual, production-weighted annual, and seasonal temperatures, they determined that the best fit between $U_{37}^{k'}$ and temperature comes from using the mean annual sea surface temperatures of overlying water.

2.3.2 Seasonality of alkenone production and $U_{37}^{k'}$

The issue of whether alkenones in surface sediments reflect the overlying water temperature is already implicit in calibration studies. That is, the relationship between the $U_{37}^{k'}$ index and sea surface temperature was defined to provide the maximum possible correlation between these two properties, and that maximum correlation was found between $U_{37}^{k'}$ and mean annual surface temperature for the popular calibration determined by Müller et al. [29]. The same study also compared $U_{37}^{k'}$ with mean annual temperature at a variety of depths, production-weighted annual mean surface temperature, and seasonal average surface temperature, all of which had lower correlation coefficients than mean annual temperature at the surface.

Prahl and coworkers [36] measured alkenone production and composition in particulate organic matter and from sediment traps at Station ALOHA in the oligotrophic North Pacific. They determined that alkenone production and export events can take place in both winter and summer, for separate reasons. They linked the summer export events to "new production" caused by nitrogen fixation in the surface mixed layer, whereas the winter events were tied to eddy-scale mixing of nutrients up from deep waters and occurred in the deep chlorophyll maximum layer. Even though the winter export events occurred deeper in the water column and at a colder temperature, $U_{37}^{k'}$ values representing a production-weighted average of summer and winter export were in agreement with mean annual sea surface temperatures. Prahl et al. therefore concluded that the seasonality of alkenone production and longer-term variations in ecology and productivity should not affect the applicability of $U_{37}^{k'}$ as a paleoclimate proxy.

2.3.3 Preservation of alkenone signal

In order to have confidence in a paleo-temperature reconstruction based on alkenone unsaturation ratios, we need to be confidant that the unsaturation pattern measured from a sediment core sample is not substantially different from the alkenone unsaturation ratio in the overlying water column at the time that sediment was deposited.

Sikes et al. [45] provide some evidence that $U_{37}^{k'}$ values do not change during routine handling and storage procedures typical for sediment cores designated for paleoceanographic studies, at least over storage periods up to four years. Thus if the signal has not been altered in the water column or sediments prior to core collection, an authentic $U_{37}^{k'}$ value can be measured.

There are several questions to answer in addressing the issue of whether sedimentary $U_{37}^{k'}$ specifically represents the temperature of overlying waters at the time the sediment was deposited. First, does the $U_{37}^{k'}$ of lipids extracted from surface sediments record the same signal as the overlying water? How does sediment redistribution affect alkenone deposition? And finally, do early diagenetic processes, and particularly oxidative degradation, alter the $U_{37}^{k'}$ composition of down-core sediments?

Prahl et al. [35] investigated preservation of alkenones in marine sediments by comparing sediment from above and below an oxidation horizon in two different cores from the same massive turbidite deposit. They found that although the concentration of alkenones in the sediments decreased by about 88% from the unoxidized to the oxidized section of the turbidite, the $U_{37}^{k'}$ values were very similar. When translated to temperature using the calibration by Prahl et al., 1988 [39], the variation of $U_{37}^{k'}$ values between oxidized and unoxidized samples corresponds to less than 1^{o}C. These results suggest that the $U_{37}^{k'}$ of sediments is not altered by exposure to oxygen (and by implication also nitrate and other weaker oxidizing agents.) Investigating the effect of carbonate dissolution on $U_{37}^{k'}$, Sikes et al. [45] found that exposure of sediments to acidic conditions in a laboratory setting did not affect $U_{37}^{k'}$ values, even when the exposure to acid was sufficient to dissolve almost all carbonate from a moderately carbonate-rich sediment. They additionally noted that offsets between U_{37}^{k}-based SST from core-top samples and measured SST of overlying waters in a global dataset were not correlated with water depth, so Sikes et al. [45] concluded that carbonate dissolution does not impact U_{37}^{k}.

2.3.4 The imperfect relationship between $U^{k'}_{37}$ and SST

Not all studies have shown $U^{k'}_{37}$ to be linearly well-correlated to mean annual sea surface temperature, particularly at low temperatures and low salinities. Some studies [4, 42] suggest that U^{k}_{37} is much better correlated than $U^{k'}_{37}$ to sea surface temperatures when those temperatures are low, particularly below about 8° C. Other work [46] has demonstrated that $U^{k'}_{37}$ can still correlate well with the low temperatures characteristic of the Southern Ocean, and that $U^{k'}_{37}$ is a better proxy than U^{k}_{37} for temperature in the Southern Ocean. A comparison between core-top U^{k}_{37} and $U^{k'}_{37}$ values at high northern and southern latitudes [42] showed that although U^{k}_{37} correlates well with SST in both hemispheres, the exact relationship differs between the Southern Ocean dataset and the Nordic Seas dataset. $U^{k'}_{37}$, on the other hand, did not show the same relationship to SST in the high northern latitudes as it had in the high southern latitudes [42]. Sites where Bendle and Rosell-Melé [4] demonstrated $U^{k'}_{37}$ and SST pairings inconsistent with the Müller et al., 1998 [29] calibration occurred almost exclusively north of 67°N in the Nordic Seas, so the Müller et al., 1998 [29] calibration should still be applicable in regions south of 67°N. The breakdown in a linear relationship between $U^{k'}_{37}$ and SST at low temperatures thus seems geographically constrained, though it does provide reason for caution when applying the proxy into the past.

Salinity also may have a significant effect on $U^{k'}_{37}$ [5], at least at the lower salinities of coastal waters. A study of alkenone production and unsaturation patterns across a salinity transect between the North Sea and the Baltic Sea showed that even though temperature, light, and nutrients were almost constant over the region, $U^{k'}_{37}$ varied significantly, and was correlated to sea surface salinity [5]. These results came from measuring both particulate organic matter from a bloom of *E. huxleyi*, a major alkenone-producing species, and alkenones extracted from surface sediments. They were able to rule out significant contributions of sedimentary alkenones from other species based on the patterns of alkenone and alkenoate compounds, so the unexpected lack of a clear relationship between $U^{k'}_{37}$ and SST could not be attributed to

an unknown alkenone producer.

In a culture study of the somewhat uncommon alkenone-producing species *Isochrysis galbana*, Versteegh and coworkers [51] determined that $U^{k'}_{37}$ values can be altered by both nutrient and light limitation, producing an apparent temperature offset around 2-3°C. Prahl and coworkers [38] cultured the ubiquitous *Emiliania huxleyi* and also determined that nutrient limitation causes $U^{k'}_{37}$ values to be too low for the given temperature, and light limitation causes $U^{k'}_{37}$ to be too high.

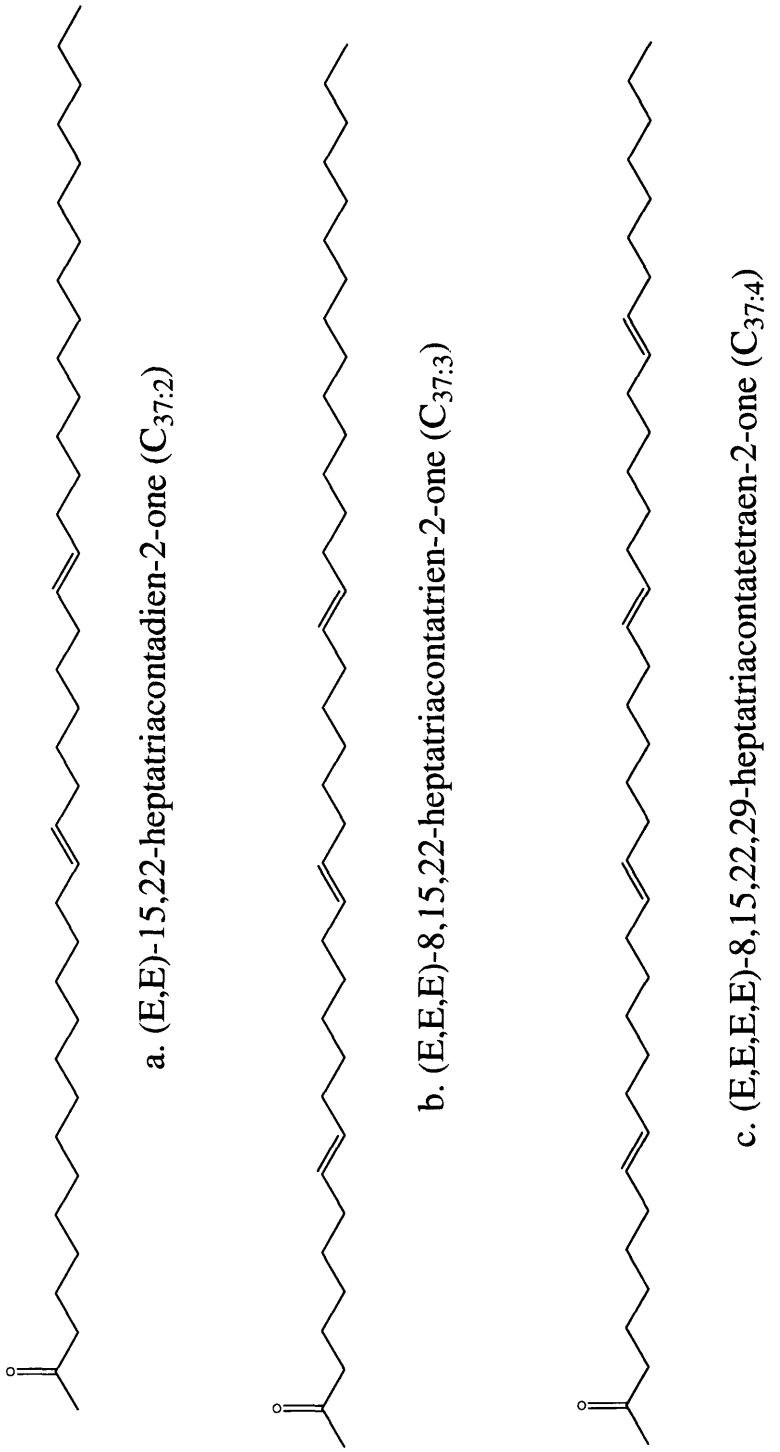

Figure 2-3: Chemical structures of the three C_{37} methyl ketones used in determining U_{37}^{k} and $U_{37}^{k'}$.

Chapter 3

Methods

3.1 Samples

Samples for alkenone analysis were collected from five available sediment cores. The gravity core 51GGC was collected from the Carolina Slope (32°47.041'N, 76°17.178'W) at 1790 m water depth on R/V Knorr Cruise 140 Leg 2 during November, 1993. On the same cruise, gravity core 39GGC was collected from the Blake Ridge (31°40.135'N, 75°24.903'W) at 2975 m water depth. Core 51GGC and 39GGC were sampled every 4 cm to a total depth of 2.9 m in core 51GGC and 1.17 m in core 39GGC. Three cores from the Marion Dufresne cruise MD101, part of the IMAGES program, were also sampled. Core MD95-2025 comes from the Orphan Basin (49.79°N, 46.7°W) at 3009 m water depth. The archive section of the Orphan Basin core was sampled every 100 cm over the top 30 m of core. Core MD95-2028 was collected from the Fogo Seamount (42.1°N, 55.75°W) in 3368 m of water. The archive section of the Fogo Seamount core was sampled every 100 cm for the first 5 m of core, every 200 cm to a depth of 19 m, and then every 100 cm again to a final depth of 22 m. Core MD95-2031 comes from a site in the Grand Banks called Narwhal (44.31°N, 53.74°W) in 1570 m of water. The Narwhal core was sampled every 20 cm from the coretop down to a maximum depth of 12 m.

Samples were taken from a 1 cm depth interval, and care was taken to exclude material that had touched the sides of the core liner and material that had been

Core number	Location	Latitude	Longitude	Water depth
KNR140-39GGC	Blake Ridge	31°41.135′N	75°24.903′W	2975 m
KNR140-51GGC	Carolina Slope	32°47.041′N	76°17.178′W	1790 m
MD95-2025	Orphan Basin	49.79°N	46.7°W	3009 m
MD95-2028	Fogo Seamount	42.1°N	55.75°W	3368 m
MD95-2031	Narwhal	44.31°N	53.74°W	1570 m

Table 3.1: Sediment cores used in this study.

exposed to the air after the core had been split. Each sample represented between 5 g and 15 g wet mass. Samples were stored frozen at -20 to -30°C in precombusted 16 ml glass vials, and then freeze-dried at -50°C using a Virtis Benchtop freeze-drier for several days, after which they were stored in a dessicator prior to lipid extraction.

3.2 Lipid Extraction

All materials were pre-combusted at 450°C or greater for at least 8 hours. All tools and equipment, including the stainless steel cells, were washed with tap water (3x) and deionized water (3x), and then either sonicated in methanol and then dichloromethane (DCM) for at least 3 minutes each, or rinsed sequentially in methanol (3x), DCM (3x), and hexanes (3x). For extraction of each sample, first 3-5 g of pre-combusted Na_2SO_4 and then 3-12 g of dry, ground-up sediment was loaded into a stainless steel cell with a similar mass of Na_2SO_4 and 20 μl of 0.103mg/ml n-C_{37} alkane in toluene internal recovery standard, glass fiber filters (VWR®, pore size 1.5 μm) on either end of the cell, and quartz sand (Accusand®) separated by another filter to fill the cell. Samples were then extracted with DCM using a DIONEX ASE 200 Accelerated Solvent Extractor. Each sample was extracted using 3 consecutive 5-minute extraction cycles at 1500 psi and 150°C. A slightly modified procedure was used to extract samples that needed to be preserved for future isotopic work on foraminifera. For these samples (roughly half of the samples from MD95-2025 and MD95-2031, and all samples from MD95-2028), the sediment was gently mixed with a spatula rather than ground, and Na_2SO_4 on either side of the sample was separated

by a glass fiber filter. These samples were extracted in the ASE at 1000 psi and 100°C.

After extraction, all samples were dried down under nitrogen using a Zymark TurboVap evaporator and stored at -20 to -30°C, if necessary. Total lipid extracts were then transferred to 2 ml borosilicate Target® vials (National Scientific®) using rinses of acetone/DCM (1:1 v:v), DCM (2x) and hexanes, and solvents were evaporated under nitrogen. Total lipid extracts were dissolved in 400 μl toluene with a known quantity of n-C_{36} alkane quantitation standard and derivatized by silylation with 10 μl bis(trimethylsilyl)trifluoroacetamide (BSTFA) at 50°C for one hour using a Pierce Reacti-Therm III™ hot plate in preparation for alkenone identification and quantification by gas chromatography.

3.3 Alkenone Quantitation

Di- and tri-unsaturated C_{37} alkenones were identified and quantified using an Agilent Technologies 6890N gas chromatograph with flame ionization detection (GC-FID). A 10 μl aliquot of the 410 μl derivatized total lipid extract solution was injected onto the 60-m-long, 0.32 mm diameter fused silica Chrompack capillary column (CP-Sil 5CB, #CP8744) using a 7683 Series injector with autosampler. Identification of n-alkane standards and alkenone peaks was made by comparison of retention time with a known sediment standard. Determination of alkenone concentrations was achieved by comparison of alkenone peak areas with the area of the n-C_{36} alkane quantitation standard.

Some samples, particularly from core MD95-2025, had very low alkenone concentrations, such that a 10 μl aliquot out of 410 μl of total lipid extract solution was insufficient to robustly determine the alkenone concentrations. After the initial quantitation and determination of low concentration, these samples were dried down under nitrogen and then re-derivatized with 2 μl BSTFA in either 20 or 40 μl of dry toluene at 50°C for one hour. A 10 μl aliquot of the 22 or 42 μl solution was then injected on the GC-FID for alkenone quantitation.

3.4 Saponification

A number of samples, particularly some with low alkenone concentrations, contained compounds whose peaks overlapped with those of the two C_{37} alkenones being measured, such that alkenone quantitation was not initially possible. Since the interfering compounds were suspected to be primarily fatty acids and alcohols with more polar moieties than the alkenone compounds of interest, those sample were hydrolyzed to separate the ketones for additional analysis.

The total lipid extracts were dissolved in 3 ml of 1N KOH in methanol and sonicated for approximately 3-4 minutes. After that, 1 ml of dichloromethane- (DCM-) extracted deionized water was added and the samples were shaken vigorously. The vials were then capped under nitrogen and allowed to sit in an oven at 60°C overnight in order for the hydrolysis reaction to proceed fully.

The polar and non-polar compounds were then separated by adding approximately 15 ml each of DCM-extracted water and hexane to the solutions. The solution was shaken vigorously and then the solvents were allowed to separate. The hexane fraction, containing the less polar compounds, was then carefully pipetted off into a separate vial. An additional 15 ml of hexanes was added 3 more times and the process repeated. The aqueous fraction, containing the more polar compounds, was saved separately.

The hexane fraction was then back-extracted using 15 ml DCM-extracted water. After vigorous shaking and subsequent settling and separation of the solvents, the hexane portion was carefully pipetted off into a new vial containing a small amount of pre-combusted sodium sulfate (Na_2SO_4), to remove any remaining water. The hexane was finally transferred to one last clean vial, and the sodium sulfate was rinsed 3 times with several milliliters of clean hexane.

The hexane fraction was finally dried down under nitrogen, then transferred to a small GC vial and re-derivatized with BSTFA, as above, for analysis by GC-FID. Samples that needed saponification are listed in Table 3.2.

Core number	Location	Depth
MD95-2025	Orphan Basin	300-301 cm
MD95-2025	Orphan Basin	400-401 cm
MD95-2025	Orphan Basin	600-601 cm
MD95-2025	Orphan Basin	1000-1001 cm
MD95-2025	Orphan Basin	1800-1801 cm
MD95-2025	Orphan Basin	2000-2001 cm
MD95-2025	Orphan Basin	2100-2101 cm
MD95-2025	Orphan Basin	2200-2201 cm
MD95-2025	Orphan Basin	2900-2901 cm
MD95-2028	Fogo Seamount	1100-1101 cm
MD95-2031	Narwhal	1080-1081 cm

Table 3.2: Samples where overlapping GC peaks in the initial analysis interfered with alkenone quantitation and necessitated saponification.

3.5 Standards

Standard solutions were used to quantify alkenone concentrations and to measure loss of the total lipid extract during transfers and processing. The internal recovery standard solution used was 0.103 mg/ml n-C_{37} alkane in toluene. The quantitation standard used was 5.122 μg/ml n-C_{36} alkane in toluene.

To measure procedural precision, a sediment standard from Bermuda Rise core GGC-5 (referred to as BRC) was measured after approximately every 10 samples. Overall precision in measuring $U_{37}^{k'}$ from the BRC standard was 0.0256 in $U_{37}^{k'}$ units, which is equivalent to 0.75°C, or less than the standard error for reconstructing temperature using a number of core-top calibrations [29]. Reproducibility of the alkenone concentration was $\pm$10% of the concentration measured.

3.6 Calculation of $U_{37}^{k'}$

The parameter $U_{37}^{k'}$, defined in Equation 2.2, was calculated as the ratio of concentrations of the two methyl ketone compounds. An alkenone-based sea surface

temperature was then calculated from the $U_{37}^{k'}$ according to:

$$U_{37}^{k'} = 0.039 + 0.034 * T \tag{3.1}$$

or alternatively,

$$T = \frac{U_{37}^{k'} - 0.039}{0.034} \tag{3.2}$$

from the *E. huxleyi* culture calibration of Prahl et al., 1988 [39].

3.7 Age Models

3.7.1 Blake Ridge, KNR140-39GGC

For core KNR140-39GGC, calibrated ^{14}C dates from planktonic foraminifera were provided by L. Keigwin (pers. comm.) as published by Keigwin and Schlegel [22]. Original radiocarbon dates were calibrated according to Stuiver et al., 1998 [48] and Bard et al., 1998 [3] by Keigwin and Schlegel, 2002 [22]. The provided dates were interpolated to the depths of alkenone measurements using the PCHIP (Piecewise-Cubic Hermite Interpolating Program) cubic spline in MATLAB to obtain the age model for that core. The age model for KNR150-39GGC is shown in Figure 3-1.

3.7.2 Carolina Slope, KNR140-51GGC

^{14}C dates from planktonic foraminifera in core KNR140-51GGC [23] were calibrated using the CALIB v. 5.0 program [49] and the Marine04 calibration [18], which assumes a 400 year offset between marine and atmospheric carbon. No core-top date was available, so a date of 0 years BP was assumed, and the dates were then interpolated to sample depths using a linear interpolation. The age model for core KNR140-51GGC is shown in Figure 3-2.

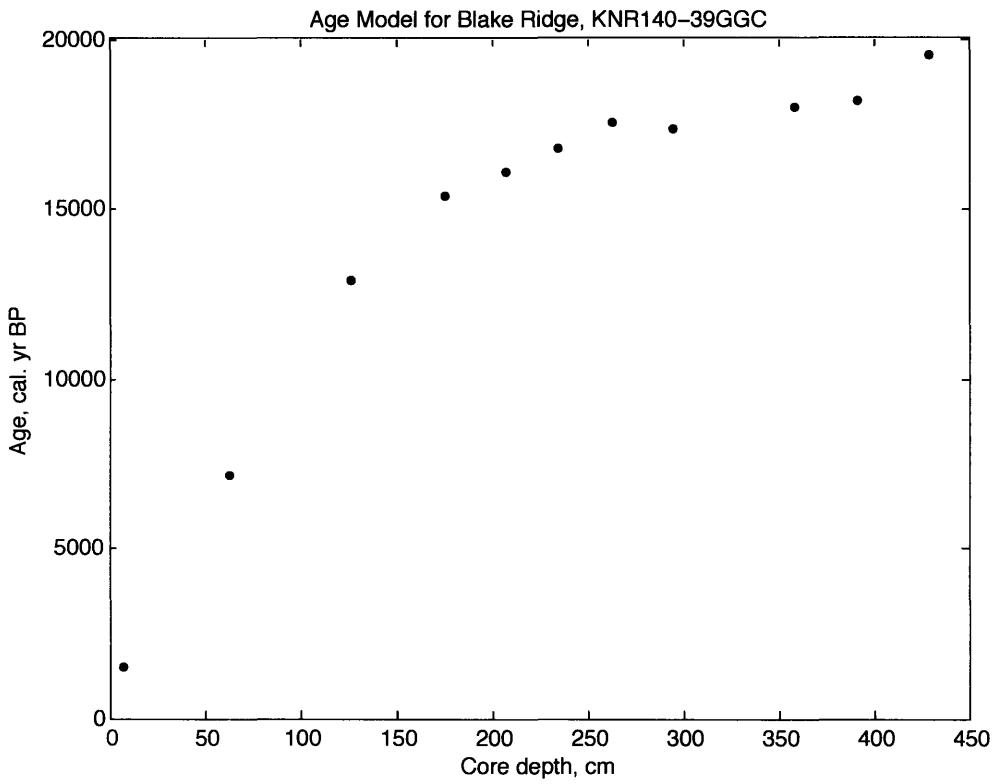

Figure 3-1: Age model for core KNR140-39GGC from the Blake Ridge in calibrated years before present. The age model used in this study was interpolated from the available radiocarbon-based dates using a PCHIP (Piecewise-Cubic Hermite Interpolating Program) spline in MATLAB. Radiocarbon dates are from foraminifera, and calibrated ages were calculated according to Stuiver et al., 1998 [48] and Bard et al., 1998 [3] by Keigwin and Schlegel, 2002 [22]. Data courtesy L. Keigwin, 2005 (pers. comm.)

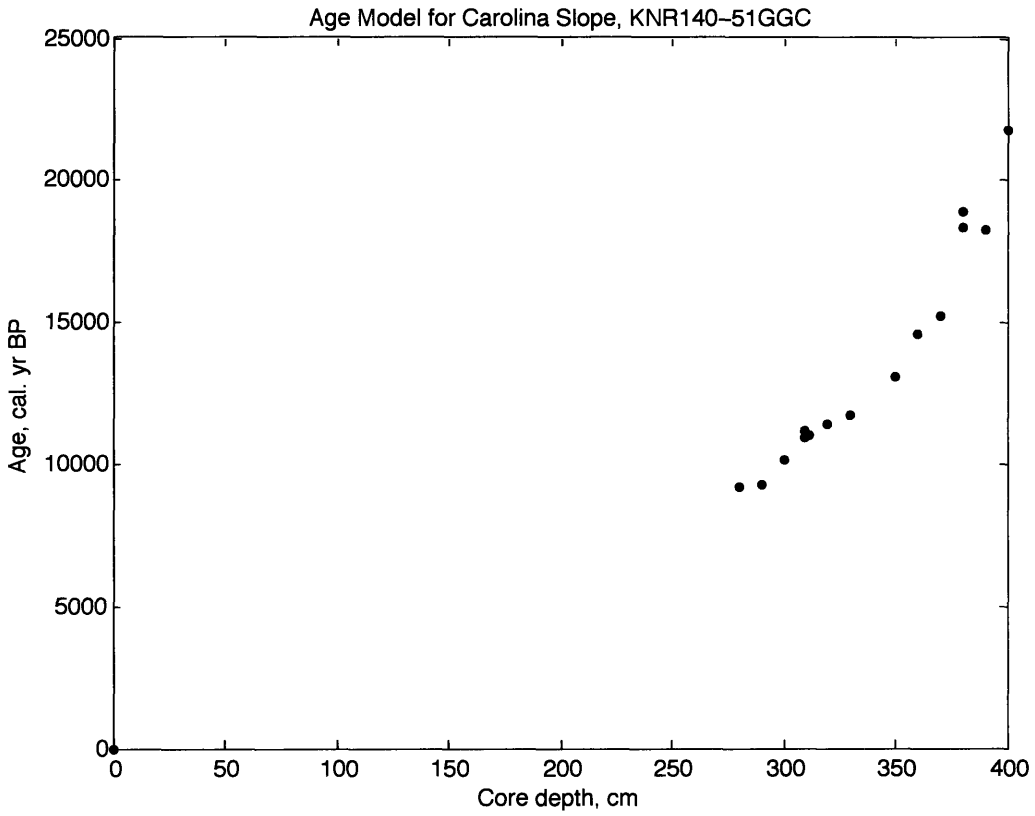

Figure 3-2: Age model for core KNR140-51GGC from the Carolina Slope in calibrated years before present. Data are from Keigwin, 2004 [23], and were converted from radiocarbon age to calibrated age using the CALIB v. 5.0 program from Stuiver et al., 2005 [49] and the Marine04 calibration dataset of Hughen et al., 2004 [18], which assumes a 400 year offset between marine and atmospheric carbon. Core-top value of 0 age is assumed, for lack of additional data. A linear interpolation was used to estimate the age-depth relationship for depths of samples.

3.7.3 MD95-2031, Narwhal

To determine an age model for this core, tests of the planktonic foraminifer *G. bulloides* were picked from the >250μm fraction and from the 150-250μm fraction of either extracted or non-extracted freeze-dried sediment after disaggregating and rinsing the sample using deionized water. Extraction at high temperature and pressure using an organic solvent has previously been shown to have no demonstrable effect on ^{14}C content of foraminifera [32]. One sample did not have sufficient *G. bulloides* for radiocarbon dating, so *N. pachyderma* (left-coiling) was picked from the 150-250 μm fraction instead. After picking, the foraminiferal tests were rinsed thoroughly in deionized water and dried in an oven at approximately 50°C. Discolored or otherwise odd-looking tests were discarded from the samples, and care was taken to remove any non-foraminiferal material from the samples. The cleaned samples were then submitted to the NOSAMS accelerator mass spectrometry facility in Woods Hole, MA for analysis. Table 3.3 lists the sample depths and species submitted. Unfortunately, age data was not available in time for inclusion in this document.

Depth	Species
2-4 cm	*G. bulloides*
190-200 cm	*G. bulloides*
396-399 cm	*G. bulloides*
580-582 cm	*N. pachyderma (s.)*
859-861 cm	*G. bulloides*
1159-1161 cm	*G. bulloides*

Table 3.3: Planktonic foraminifera samples submitted to NOSAMS for dating.

3.7.4 MD95-2028, Fogo Seamount

No age information was available for MD95-2028, and after preliminary alkenone data were obtained, it was determined that developing an age model at this site would be beyond the scope of this study.

3.7.5 MD95-2025, Orphan Basin

The age model for MD95-2025 comes from data published in Hiscott et al., 2001 [17]. The information from that reference used here includes four radiocarbon dates from mixed planktonic foraminifera, one age for an ash layer, and a depth for the Marine Isotope Stage (MIS) 5/6 transition visually estimated from a plot of $\delta^{18}O$. The ash layer at 9.70 m was determined by Hiscott et al. to be the 57.5 ka Ash 2 from Ruddiman and McIntyre, 1984 [43]. The age of the MIS 5/6 transition was taken from Imbrie et al., 1984 [20] to be 127 ky B.P. The ages of the two younger radiocarbon samples from Hiscott et al. were calibrated for this study using the CALIB v. 5.0 program from Stuiver et al., 2005 [49] and the Marine04 calibration dataset of Hughen et al., 2004 [18], which assumes a 400 year offset between marine and atmospheric carbon. The other two radiocarbon ages given were too old to use the Stuiver et al. [49] program or the Hughen et al. [18] datasets, and were left in uncalibrated radiocarbon years, for which Hiscott and coworkers [17] used a 5568 year half-life for ^{14}C and assumed no reservoir correction. Little difference was noticed in the overall age model after changing the younger two ages from radiocarbon years to calibrated years.

A core-top age of 0 years B.P. was assumed, since no age above 60 cm was given. However, a sample of *G. bulloides* was picked from the 0-1 cm sample taken for this study. That sample was prepared as the other foraminifera samples listed for MD95-2031 (Narwhal) and was also submitted to NOSAMS in Woods Hole for AMS dating, but unfortunately that data was not available in time for inclusion in this document.

The specific data used in the age model for MD95-2025 are listed in Table 3.4 and are depicted in Figure 3-3. Specific ages for sample depths were determined by linear

interpolation and extrapolation from the data points shown.

Depth	Data type	Age (^{14}C years BP)	Age (cal. years BP)	Standard error	Source
0 cm	assumed	-	0	N.A.	this study
60-62 cm	mixed plank. forams	6260	6712	70	[17]
230-232 cm	mixed plank. forams	12470	13913	90	[17]
420-422 cm	mixed plank. forams	22510	-	180	[17]
640-642 cm	mixed plank. forams	28960	-	270	[17]
970 cm	ash layer	-	57,500	-	[17, 43]
1825 cm	MIS5/6 transition in δ^{18}O	-	127,000	-	[17, 20]

Table 3.4: Age model data for MD95-2025, Orphan Basin.

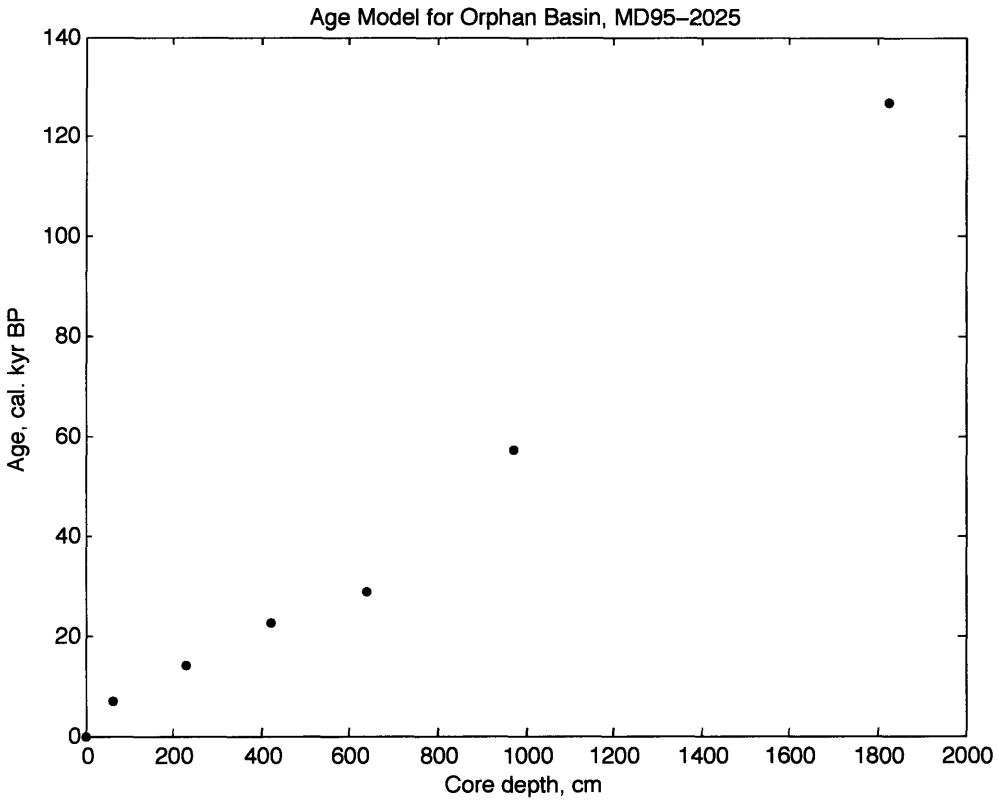

Figure 3-3: Age model for core MD95-2025 from the Orphan Basin, in calibrated years before present. Data and their sources are listed in Table 3.4. A linear interpolation and extrapolation was used to determine ages for each sample used for alkenone measurement.

Chapter 4

Results

Alkenone concentration and ratio data were obtained from 5 separate sediment cores from the northwest Atlantic, listed in Table 3.1 and shown in their geographic and bathymetric context in Figure 4-1. These locations span a wide range of latitude and are generally located along the continental slope.

Alkenone-based temperatures from the two sites south of Cape Hatteras, where the Gulf Stream separates from the slope and heads out to sea, show fairly steady temperatures over the Holocene, with ranges of only a few degrees Celsius at the Blake Ridge and Carolina Slope locations. The sites farther north show considerably more variation, though it was determined through alkenone analysis and subsequent research that our samples from only one of the other three sites, Narwhal (MD95-2031), represent the Holocene portion of the core. Data from the two remaining cores, MD95-2028 (Fogo Seamount) and MD95-2025 (Orphan Basin) will nonetheless be presented and discussed here, though few conclusions can be drawn from them that are specifically relevant to the Holocene temperature problem.

4.1 KNR140-39GGC, Blake Ridge

Concentrations of both the di- and tri-unsaturated C_{37} methyl ketones from the Blake Ridge samples were sufficient for good quantitation by GC-FID. The combined concentration of both compounds and the $U^{k'}_{37}$ values are shown in Figure 4-2. These

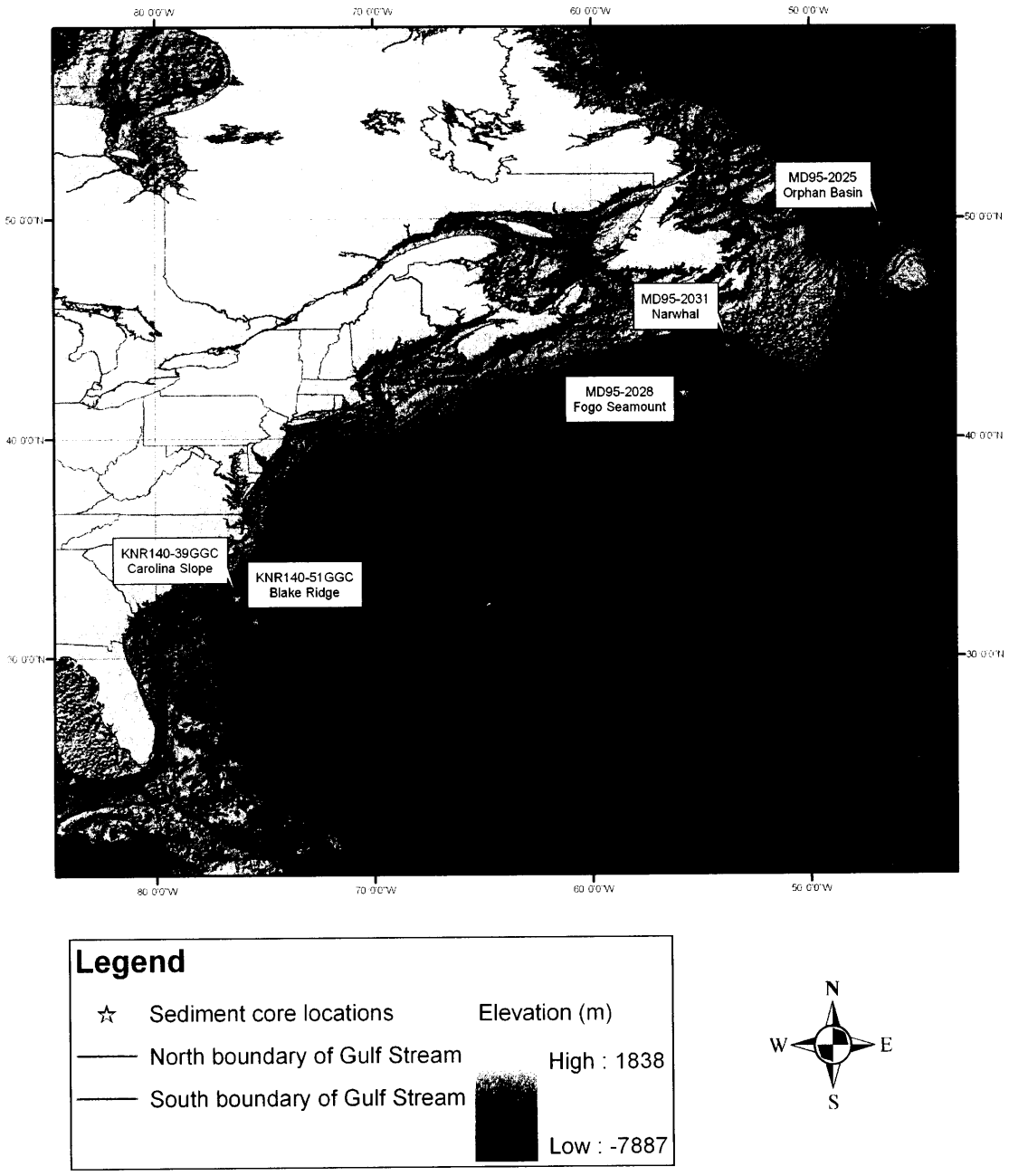

Figure 4-1: Map of the northwest Atlantic highlighting sediment core locations. Sediment core locations are listed in Table 3.1. Contour lines show 0 m, 500 m, 1000 m, 2000 m, and 3000 m below mean sea level. Gulf Stream boundaries shown delineate the 1σ (68.3%) confidence interval of the Gulf Stream position determined from satellite data [24].

parameters are uncorrelated, with a correlation coefficient of -0.0187 that is not statistically significant.

With the exception of a few outliers, the alkenone temperatures measured from the Blake Ridge are within a 2°C range for the entire Holocene. Figure 4-3 shows the sea surface temperature record, calculated from $U_{37}^{k'}$ according to Equation 3.2 from Prahl et al., 1988 [39], versus both depth and age. The age model for this core was presented in Section 3.7.1. It should be recalled that age control was sparse for this section of the core, and the age model was constructed by assuming an age of 0 years B.P. for the core-top and interpolating from the calibrated age of 9175 years B.P. at 280 cm depth.

The modern mean sea surface temperature at this location is 23.9°C [25], which is within error of the alkenone SST nearest to core-top (the top of this core was disturbed, so a core-top sample sufficient for alkenone analysis could not be obtained). However, it should be noted that the measured modern SST is slightly higher than mean Holocene SST at this site. Additionally, since age control is poor for the upper portion of this core, a lack of perfect agreement between modern and near-core-top SST is not surprising.

4.2 KNR140-51GGC, Carolina Slope

Concentration of di- and tri-unsaturated alkenones and $U_{37}^{k'}$ from the Carolina Slope are shown in Figure 4-4. Alkenone concentrations are highest near the core-top (except for one seemingly anomalous point around 230 cm depth), and there is no obvious pattern of variation in concentration. Though there is no visually obvious relationship between concentration and $U_{37}^{k'}$, the correlation coefficient between them is -0.3250, which is significant at the 95% confidence level.

Similar to the Blake Ridge, the alkenone temperatures from the Carolina Slope shown in Figure 4-5 have a range of about 2°C over the Holocene. A clear drop in temperatures is evidenced by the alkenone data between 3000 and 2000 years B.P., after which the alkenone SST returns to its previous value.

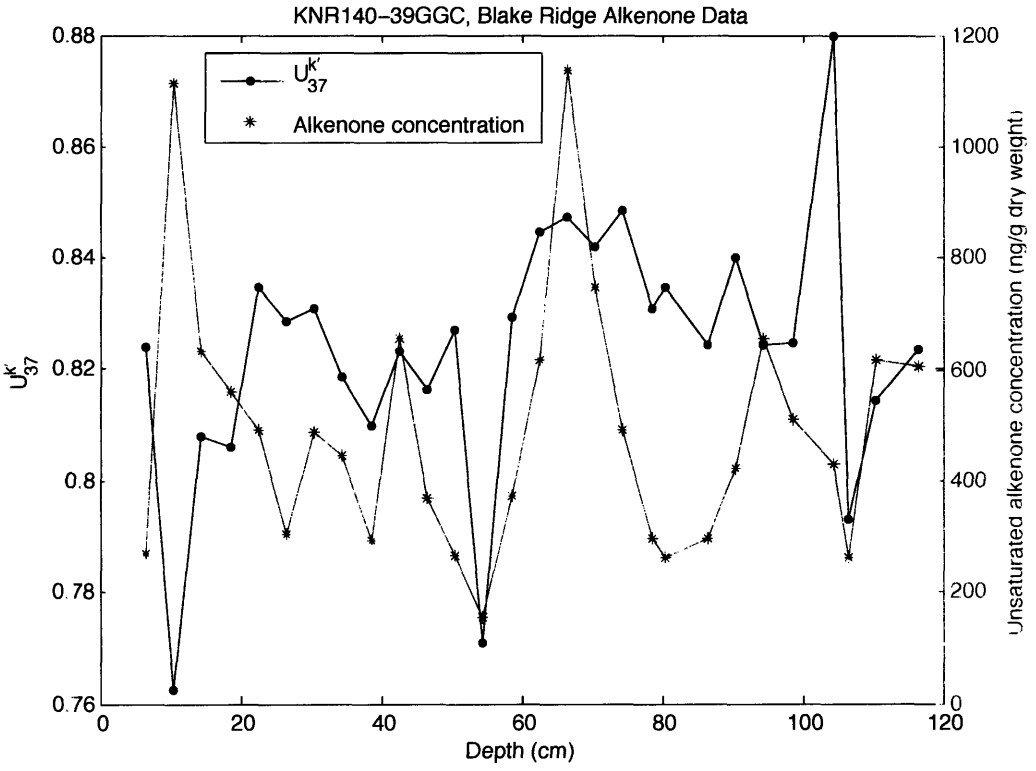

Figure 4-2: Values of alkenone unsaturation parameter $U^{k'}_{37}$ and combined concentration of $C_{37:2}$ and $C_{37:3}$ alkenones in core KNR140-39GGC from the Blake Ridge.

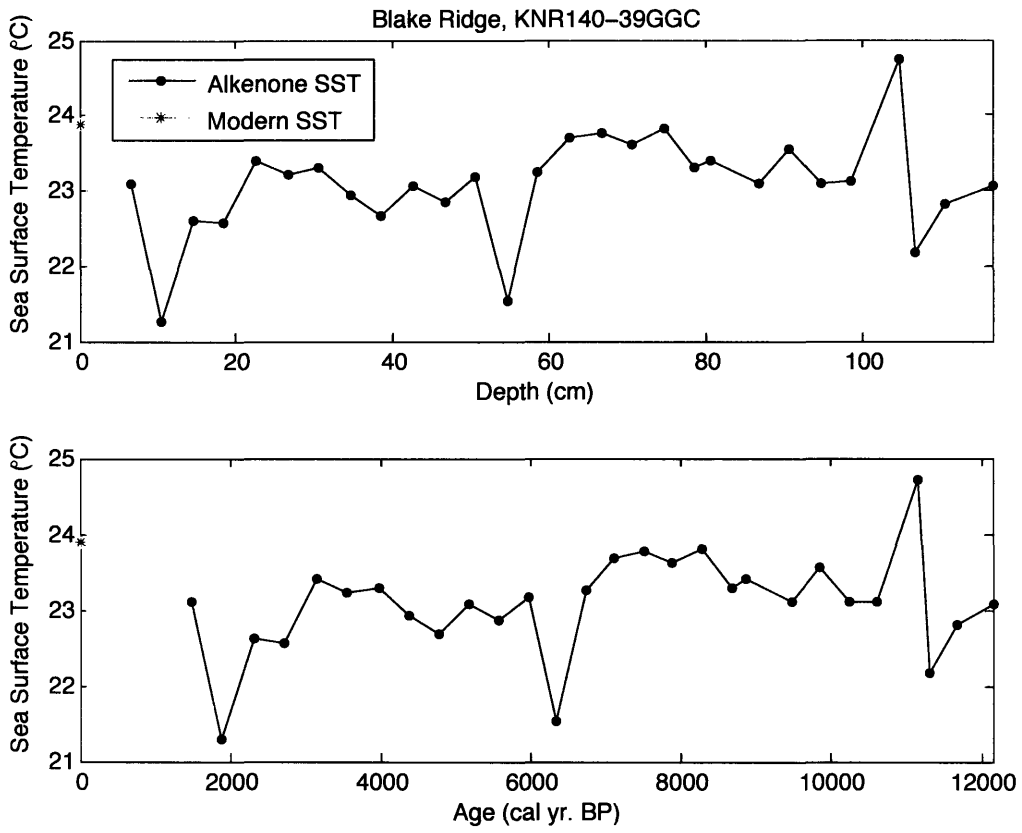

Figure 4-3: Alkenone-based sea surface temperatures for core KNR140-39GGC from the Blake Ridge. The modern sea surface temperature is from the LEVITUS94 dataset [25]. The age model used in lower panel is shown in Figure 3-1.

Depth (cm)	$U_{37}^{k'}$	SST (°C)	Concentration (ng/gdw)
6.5	0.824	23.1	269
10.5	0.762	21.3	1115
14.5	0.808	22.6	633
18.5	0.806	22.6	559
22.5	0.835	23.4	492
26.5	0.829	23.2	305
30.5	0.831	23.3	487
34.5	0.819	22.9	446
38.5	0.810	22.7	294
42.5	0.823	23.1	654
46.5	0.816	22.9	369
50.5	0.827	23.2	266
54.5	0.771	21.5	154
58.5	0.830	23.3	372
62.5	0.845	23.7	619
66.5	0.847	23.8	1139
70.5	0.842	23.6	748
74.5	0.849	23.8	489
78.5	0.831	23.3	295
80.5	0.835	23.4	263
86.5	0.824	23.1	296
90.5	0.840	23.6	421
94.5	0.824	23.1	656
98.5	0.825	23.1	511
104.5	0.880	24.7	428
106.5	0.793	22.2	260
110.5	0.814	22.8	616
116.5	0.824	23.1	606

Table 4.1: Alkenone data from KNR140-39GGC, Blake Ridge. Depth shown is the mean depth of a 1-cm-wide slice. Temperature was calculated according to Equation 3.2 from Prahl et al., 1988 [39]. Unsaturated alkenone concentration is the sum of $C_{37:2}$ and $C_{37:3}$ concentrations, in nanograms of alkenone per gram dry weight of sediment.

At this location, the modern mean SST of 23.8°C [25] agrees very well with the core-top alkenone temperature.

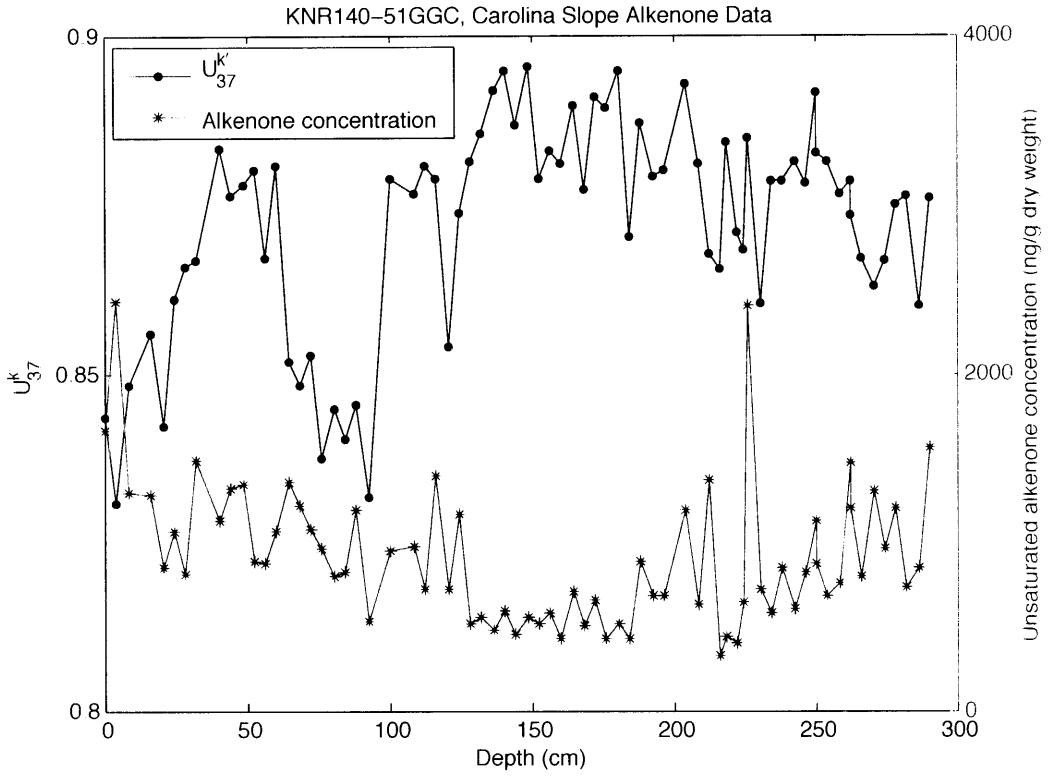

Figure 4-4: Values of alkenone unsaturation parameter $U^{k'}_{37}$ and combined concentration of $C_{37:2}$ and $C_{37:3}$ alkenones in core KNR140-51GGC from the Carolina Slope.

4.3 MD95-2028, Fogo Seamount

The concentrations of C_{37} methyl ketones at the Fogo Seamount are considerably lower than at either of the KNR140 cores farther south. The total $C_{37:2}$ and $C_{37:3}$ concentration is shown along with measured $U^{k'}_{37}$ values in Figure 4-6. The alkenone concentration and unsaturation parameter appear to be anti-correlated in this core and indeed their correlation coefficient is -0.6429, which is significant at the 95% confidence level.

The record of sea surface temperatures computed from $U^{k'}_{37}$ is shown in Figure 4-7.

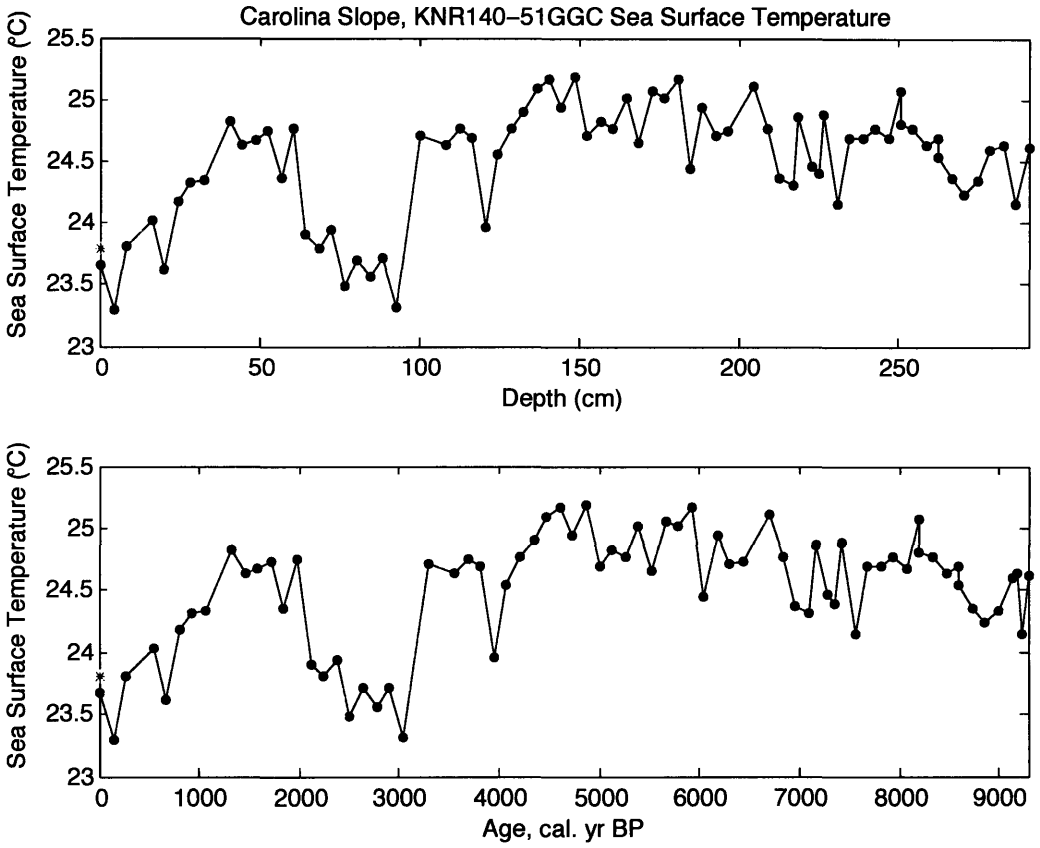

Figure 4-5: Alkenone-based sea surface temperatures for core KNR140-51GGC from the Carolina Slope. The modern sea surface temperature is from the LEVITUS94 dataset [25]. The age model used in lower panel is shown in Figure 3-2.

Depth (cm)	$U^{k'}_{37}$	SST (°C)	Concentration (ng/gdw)
6.5	0.824	23.1	269
10.5	0.762	21.3	1115
14.5	0.808	22.6	633
18.5	0.806	22.6	559
22.5	0.835	23.4	492
26.5	0.829	23.2	305
30.5	0.831	23.3	487
34.5	0.819	22.9	446
38.5	0.810	22.7	294
42.5	0.823	23.1	654
46.5	0.816	22.9	369
50.5	0.827	23.2	266
54.5	0.771	21.5	154
58.5	0.830	23.3	372
62.5	0.845	23.7	619
66.5	0.847	23.8	1139
70.5	0.842	23.6	748
74.5	0.849	23.8	489
78.5	0.831	23.3	295
80.5	0.835	23.4	263
86.5	0.824	23.1	296
90.5	0.840	23.6	421
94.5	0.824	23.1	656
98.5	0.825	23.1	511
104.5	0.880	24.7	428
106.5	0.793	22.2	260
110.5	0.814	22.8	616
116.5	0.824	23.1	606

Table 4.2: Alkenone data from KNR140-51GGC, Carolina Slope. Depth shown is the mean depth of a 1-cm-wide slice. Temperature was calculated according to Equation 3.2 from Prahl et al., 1988 [39]. Unsaturated alkenone concentration is the sum of $C_{37:2}$ and $C_{37:3}$ concentrations, in nanograms of alkenone per gram dry weight of sediment.

The temperature here appears to have varied considerably, though with no age model information, it is difficult to put this record into a historical context.

The core-top temperature at this site is 4°C warmer than the modern mean value of 13.7°C [25]. With only widely-spaced samples and no age control, it is possible that the sedimentation rate at this site is sufficiently low that the shallowest available sample at 1-2 cm is from the middle Holocene. The higher temperature of this sample compared to the modern value indicates that the most recent trend at this location has been cooling, though the timing of that cooling cannot be constrained. However, we can conclude that the cooling magnitude was no less than 4°C. If the core-top to modern cooling trend does indicate the Holocene cooling seen at nearby sites [44], then the temperature maxima near 500 cm and 2000 cm could correlate to marine isotope stages 5e and 7, respectively.

There are several other plausible explanations for the discrepancy between core-top and modern temperatures that need to be considered. The difference could be caused by advection of fine-grained sediment, and associated alkenones, from a location with a warmer temperature. However, it is not likely that advection could account for such a large difference in temperature, since both the core-top alkenone value and the modern mean value represent long-term means, and temperature gradients in this area are not large enough to explain a 4°C offset over long periods.

Since the Fogo Seamount is not very far away from the one-sigma boundary of the modern Gulf Stream, a small decrease in the number of warm-core rings between the time period represented by the core-top sample, which may be several hundred to several thousand years ago, and the modern measurements is reasonable. A decrease over centuries of the number of warm-core rings specifically affecting this location is both plausible and consistent with the difference between core-top and modern temperature, and provides one possible explanation for an observed decrease in mean annual temperature.

Another possibility to explain the core-top to modern temperature difference is that bioturbation could mix up deeper sediment, but this would account for the higher temperature only if the sediment below 1-2 cm represents a warmer temperature still

than the core top; this scenario would still be consistent with a Holocene cooling at this site. Non-thermal effects on the $U_{37}^{k'}$ value could only account for 1-3°C difference [38], and only if the organisms were exposed to physically unrealistic light limitation where their growth would be very limited. The possibility always exists that the sediment-water interface was disrupted and lost during coring, such that the core-top sample represents a time older than the Holocene.

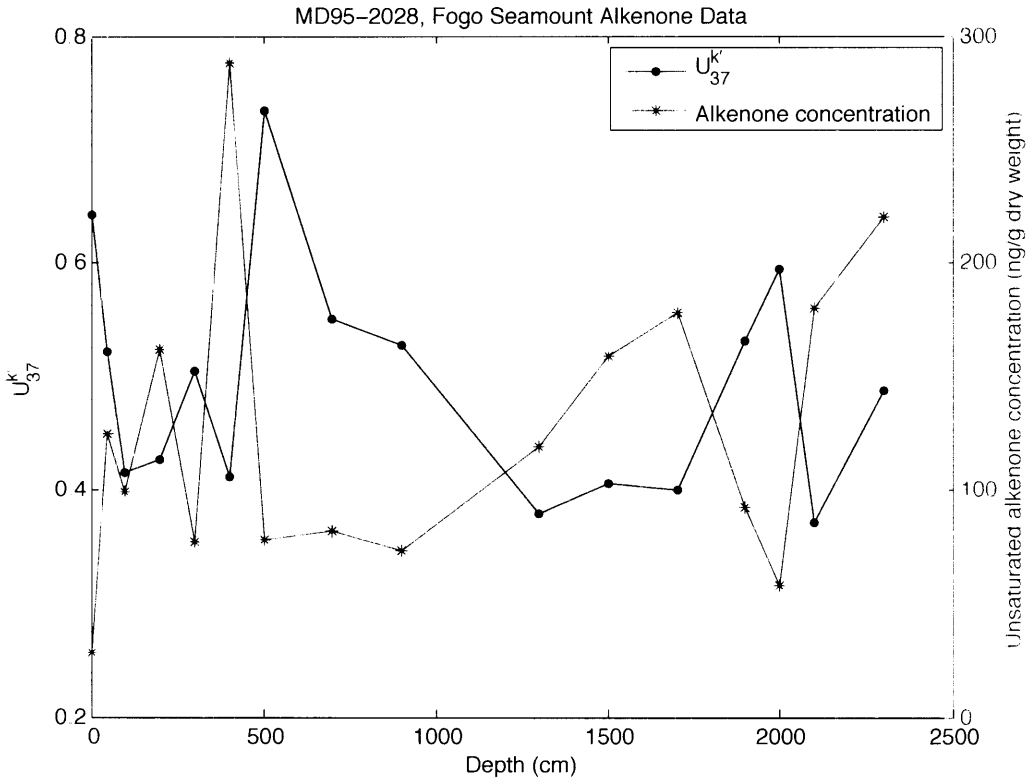

Figure 4-6: Values of alkenone unsaturation parameter $U_{37}^{k'}$ and combined concentration of $C_{37:2}$ and $C_{37:3}$ alkenones in core MD95-2028 from the Fogo Seamount.

4.4 MD95-2031, Narwhal

Alkenone concentration and unsaturation data for Narwhal are shown in Figure 4-8. As with Fogo Seamount, the two parameters appear to be anti-correlated at the

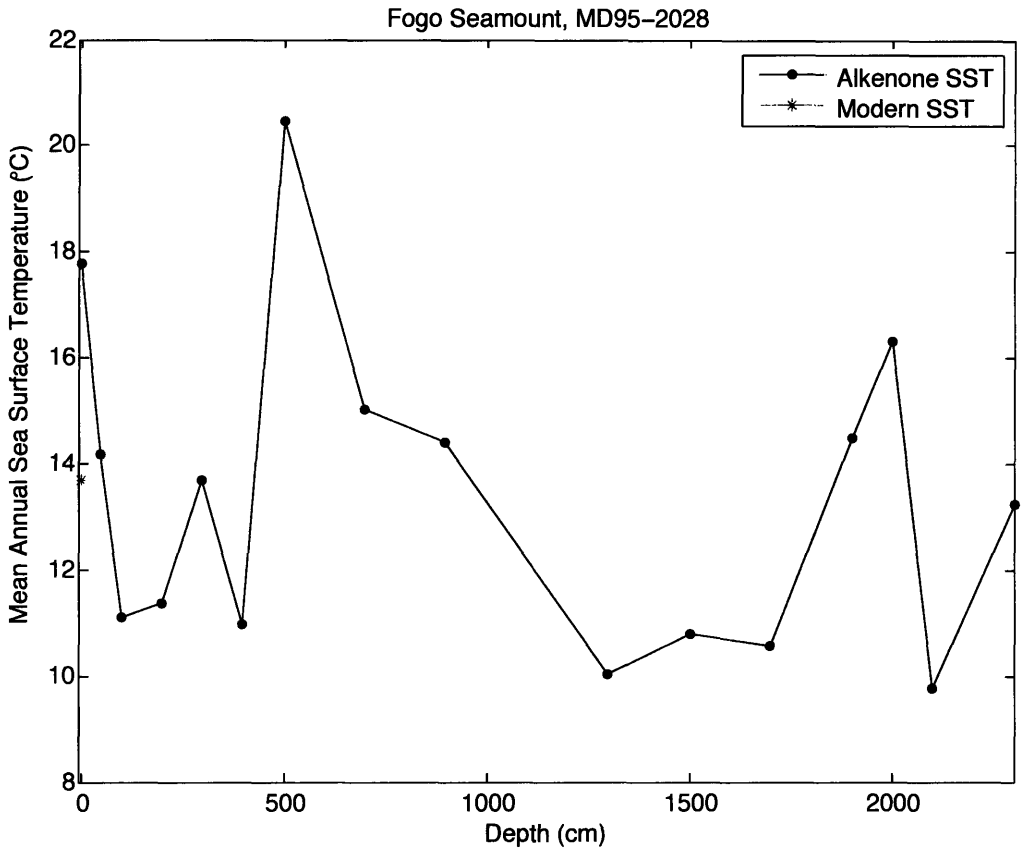

Figure 4-7: Alkenone-based sea surface temperatures for core MD95-2028 from the Fogo Seamount. The modern sea surface temperature is from the LEVITUS94 dataset [25].

Depth (cm)	$U^{k'}_{37}$	SST (°C)	Concentration (ng/gdw)
1.5	0.643	17.8	28
50.5	0.521	14.2	125
100.5	0.416	11.1	99
200.5	0.426	11.4	162
300.5	0.504	13.7	76
400.5	0.411	10.9	288
500.5	0.734	20.5	78
700.5	0.550	15.0	81
900.5	0.529	14.4	73
1300.5	0.379	10.0	119
1500.5	0.406	10.8	159
1700.5	0.399	10.6	178
1900.5	0.532	14.5	93
2000.5	0.594	16.3	57
2100.5	0.371	9.8	180
2300.5	0.488	13.2	220

Table 4.3: Alkenone data for MD95-2028, Fogo Seamount. Depth shown is the mean depth of a 1-cm-wide slice. Temperature was calculated according to Equation 3.2 from Prahl et al., 1988 [39]. Unsaturated alkenone concentration is the sum of $C_{37:2}$ and $C_{37:3}$ concentrations, in nanograms of alkenone per gram dry weight of sediment.

Narwhal location, and their correlation coefficient is a significant -0.9159. Alkenone concentrations at this site are quite high, particularly at the core-top.

The temperature record from this site, shown in Figure 4-9, shows a very consistent pattern with large variability, most notably including a decline of around 9°C from 400 cm to the core-top. At this site, an age model is not yet available, so the timeframe of these changes is not known. However, given that the most recent trend at Narwhal is a decline in temperatures, the most reasonable interpretation is that this is a Holocene record consistent with other regional observations of Holocene cooling in the Emerald Basin and Laurentian Fan [21, 44]. Further analysis of this temperature record is based on the assumption that this site records a Holocene cooling of uncertain timing.

In stark contrast to the Fogo Seamount, the core-top alkenone temperature at Narwhal is more than 3°C lower than the modern mean value of 9.2°C [25] at that site. The difference between core-top and modern temperatures therefore cannot reflect a partially missing or compressed record of monotonic cooling at this site. However, unlike the Fogo Seamount, which is located a considerable distance off-shore, the Narwhal site is located directly on the slope, so it is reasonable to expect that some down-slope sediment transport could bring material to this location that reflects cooler temperatures to the north. The possibilities that the core-top was disturbed during coring, or that the alkenone unsaturation parameter does not accurately reflect mean annual temperature in this part of the core cannot be ruled out. Bioturbation could not explain the discrepancy, because material below the core-top records a higher temperature, not lower.

4.5 MD95-2025, Orphan Basin

Alkenone concentrations at the Orphan Basin were particularly low, such that additional concentration of the extracts was necessary in many cases to quantify them. Accordingly, the uncertainty in $U_{37}^{k'}$ and alkenone concentration data is somewhat greater for this core. Data for the Orphan Basin are shown in Figure 4-10. In sharp

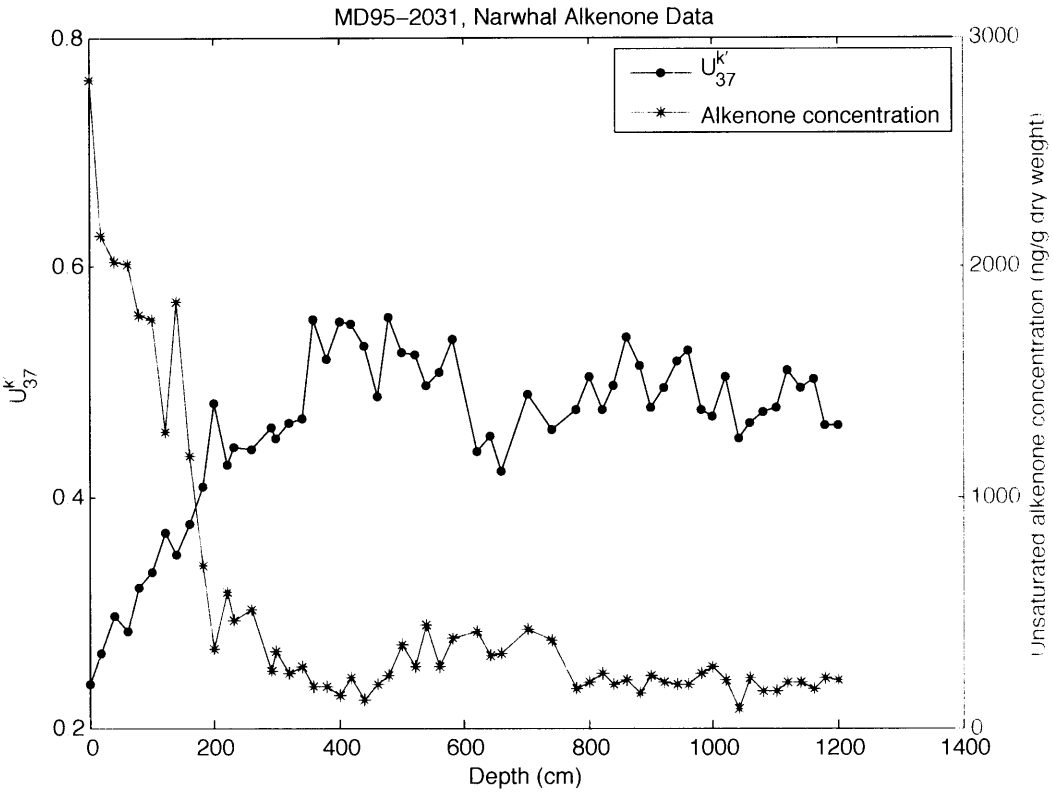

Figure 4-8: Values of alkenone unsaturation parameter $U^{k'}_{37}$ and combined concentration of $C_{37:2}$ and $C_{37:3}$ alkenones in core MD95-2031 from Narwhal.

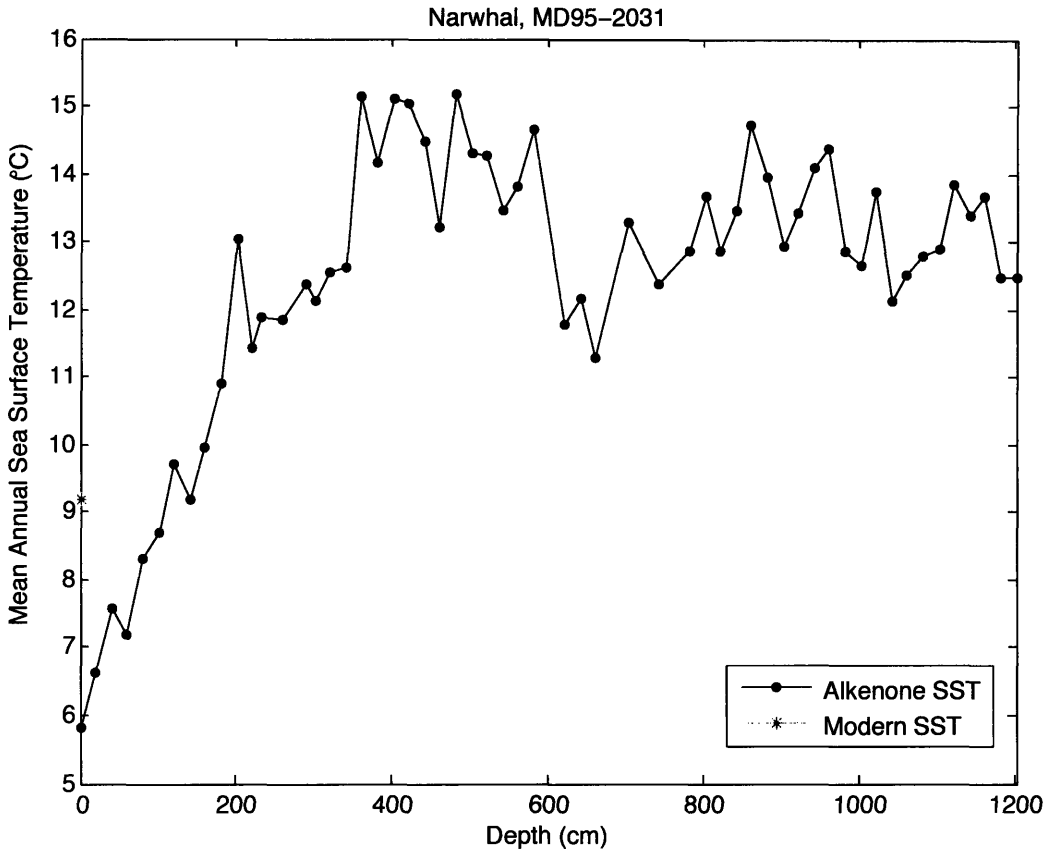

Figure 4-9: Alkenone-based sea surface temperatures for core MD95-2031 from Narwhal. The modern sea surface temperature is from the LEVITUS94 dataset [25].

Depth (cm)	$U_{37}^{k'}$	SST (°C)	Concentration (ng/gdw)
0.5	0.237	5.8	2817
20.5	0.265	6.6	2138
40.5	0.297	7.6	2017
60.5	0.283	7.2	2015
80.5	0.322	8.3	1792
100.5	0.334	8.7	1771
120.5	0.369	9.7	1288
140.5	0.351	9.2	1853
160.5	0.377	9.9	1181
180.5	0.409	10.9	703
200.5	0.483	13.0	341
220.5	0.428	11.4	592
230.5	0.443	11.9	462
260.5	0.442	11.8	513
290.5	0.460	12.4	247
300.5	0.451	12.1	329
320.5	0.465	12.5	232
340.5	0.469	12.6	266
360.5	0.554	15.1	179
380.5	0.520	14.1	180
401.5	0.553	15.1	135
420.5	0.550	15.0	211
440.5	0.531	14.5	118
460.5	0.488	13.2	186
480.5	0.556	15.2	220
500.5	0.526	14.3	358
520.5	0.524	14.3	262
540.5	0.497	13.5	440
560.5	0.509	13.8	261
580.5	0.537	14.6	386
620.5	0.440	11.8	412
640.5	0.453	12.2	313
660.5	0.423	11.3	316
700.5	0.490	13.3	425
740.5	0.459	12.4	381
780.5	0.477	12.9	166
800.5	0.504	13.7	191

Table 4.4: Alkenone data for MD95-2031, Narwhal. Depth shown is the mean depth of a 1-cm-wide slice. Temperature was calculated according to Equation 3.2 from Prahl et al., 1988 [39]. Unsaturated alkenone concentration is the sum of $C_{37:2}$ and $C_{37:3}$ concentrations, in nanograms of alkenone per gram dry weight of sediment. This dataset is continued in Table 4.5

Depth (cm)	$U_{37}^{k'}$	SST (°C)	Concentration (ng/gdw)
820.5	0.476	12.9	234
840.5	0.497	13.5	185
860.5	0.539	14.7	203
880.5	0.513	14.0	151
900.5	0.478	12.9	220
920.5	0.496	13.4	194
940.5	0.518	14.1	190
960.5	0.528	14.4	187
980.5	0.476	12.9	234
1000.5	0.470	12.7	261
1020.5	0.506	13.7	204
1040.5	0.451	12.1	79
1060.5	0.464	12.5	216
1080.5	0.474	12.8	155
1100.5	0.477	12.9	157
1120.5	0.510	13.9	199
1140.5	0.494	13.4	192
1160.5	0.503	13.7	165
1180.5	0.463	12.5	218
1200.5	0.464	12.5	210

Table 4.5: Alkenone data for MD95-2031, Narwhal, continued from Table 4.4. Depth shown is the mean depth of a 1-cm-wide slice. Temperature was calculated according to Equation 3.2 from Prahl et al., 1988 [39]. Unsaturated alkenone concentration is the sum of $C_{37:2}$ and $C_{37:3}$ concentrations, in nanograms of alkenone per gram dry weight of sediment.

contrast to the other cores examined in this study, which all showed either a negative or no significant correlation between $U_{37}^{k'}$ and concentration, the two alkenone parameters appear to be positively correlated in this core. Their correlation coefficient is 0.7282, which is statistically significant. It appears that the strength of that correlation may depend strongly on the shallowest three points, all of which contained compounds that interfered somewhat with the alkenone signal on the GC trace and thus should be regarded as less certain. However, the correlation of the two datasets, neglecting entirely those first three points, is still significant at the 95% confidence level, though the correlation coefficient of 0.5272 is considerably lower.

The corresponding temperature record from core MD95-2025 is shown in Figure 4-11. Except for the three shallowest data points, the alkenone data from Orphan Basin indicates less temperature variability than at the Narwhal site farther south, but greater variability than the two southern-most locations. The temperature range excluding the three top points is 4°C, and 9°C including those points. Note that this latter range is quite comparable with the range observed for the Narwhal core to the south. However, based on the radiocarbon dates from Hiscott and coworkers [17], which provide fairly good age control near the alkenone temperature peak, that maximum temperature measured in this record occurs around 20 kyr before present. An age of 20 kyr is very close to the convenientially recognized "Last Glacial Maximum" (LGM), and corresponds to a maximum in global ice volume [20]. It is thus highly unlikely that this peak in alkenone temperature corresponds to a true maximum temperature, and disregard of the top three datapoints on the basis of their high uncertainty is prudent. As no reliable core-top alkenone data could be obtained, a comparison with the modern mean SST value of 9.7°C [25] at this site is not possible.

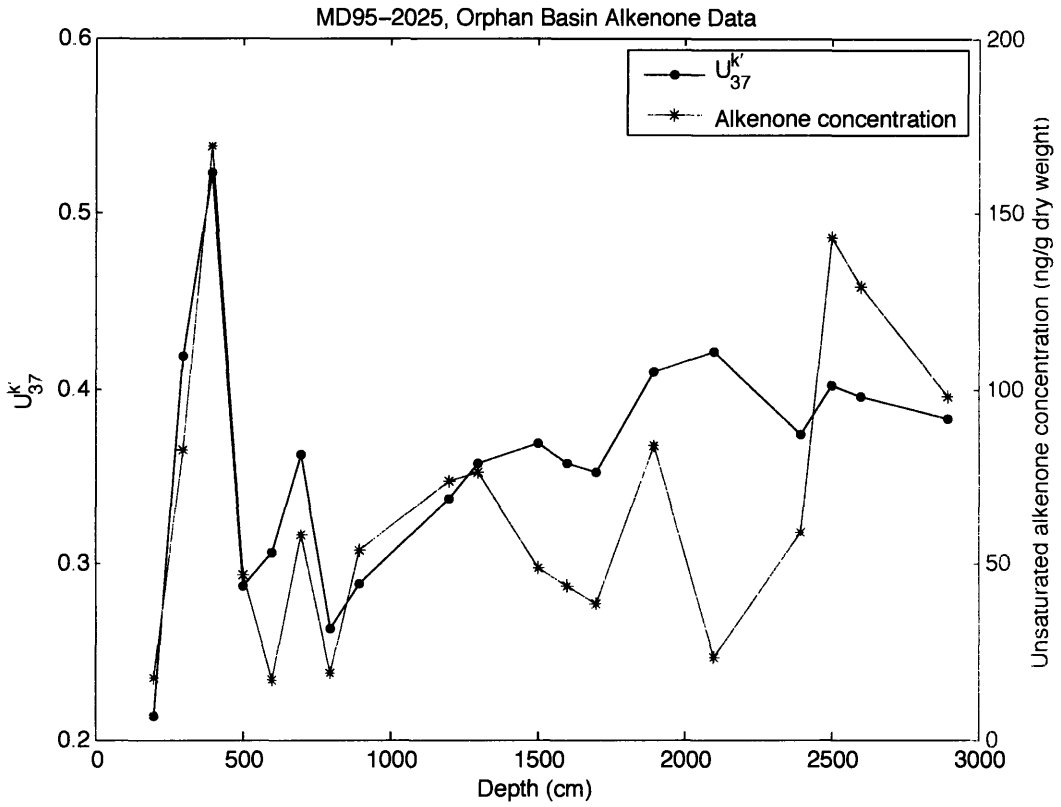

Figure 4-10: Values of alkenone unsaturation parameter $U^{k'}_{37}$ and combined concentration of $C_{37:2}$ and $C_{37:3}$ alkenones in core MD95-2025 from the Orphan Basin.

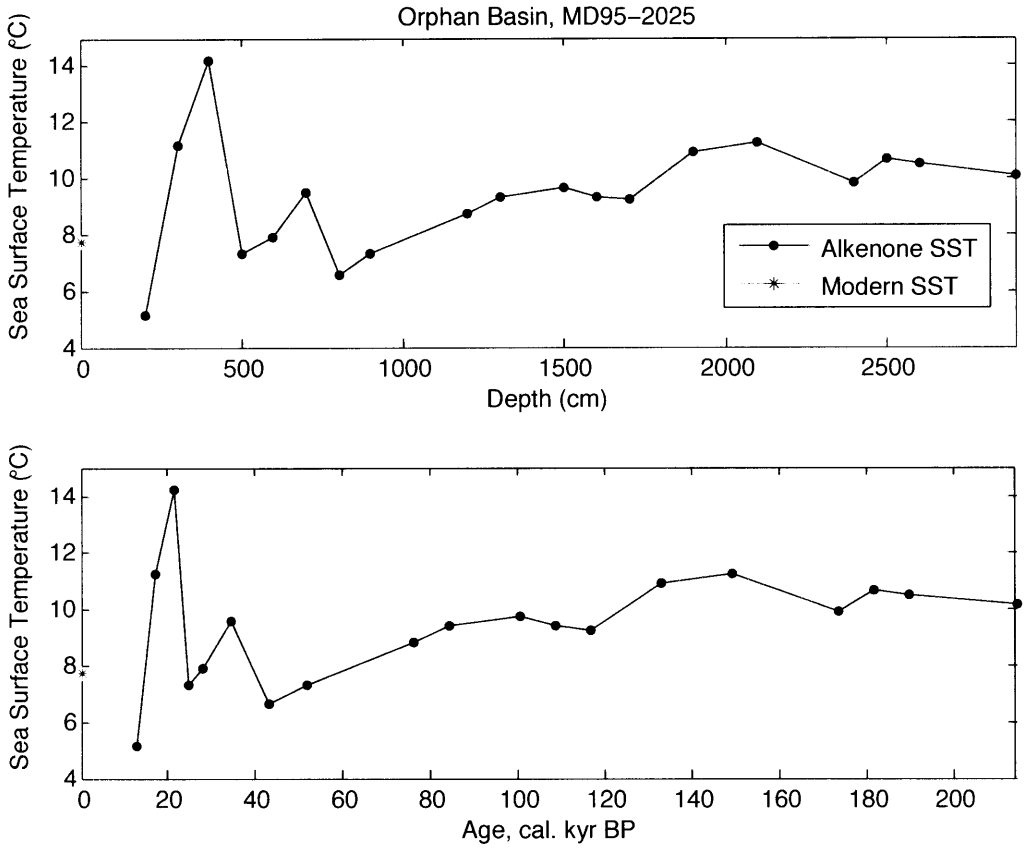

Figure 4-11: Alkenone-based sea surface temperatures for core MD95-2025 from the Orphan Basin. The modern sea surface temperature is from the LEVITUS94 dataset [25]. The age model used in lower panel is shown in Figure ??.

Depth (cm)	$U_{37}^{k'}$	SST (°C)	Concentration (ng/gdw)
200.5	0.213	5.1	17.4
300.5	0.419	11.2	82.7
400.5	0.523	14.2	169.2
500.5	0.288	7.3	46.6
600.5	0.307	7.9	16.7
700.5	0.363	9.5	58.1
800.5	0.263	6.6	18.9
900.5	0.288	7.3	53.6
1200.5	0.337	8.8	73.5
1300.5	0.358	9.4	76.2
1500.5	0.369	9.7	48.8
1600.5	0.357	9.4	43.9
1700.5	0.352	9.2	38.4
1900.5	0.410	10.9	83.9
2100.5	0.421	11.2	23.1
2400.5	0.374	9.9	59.2
2500.5	0.401	10.7	142.9
2600.5	0.396	10.5	128.9
2900.5	0.383	10.1	97.7

Table 4.6: Alkenone data for MD95-2025, Orphan Basin. Depth shown is the mean depth of a 1-cm-wide slice. Temperature was calculated according to Equation 3.2 from Prahl et al., 1988 [39]. Unsaturated alkenone concentration is the sum of $C_{37:2}$ and $C_{37:3}$ concentrations, in nanograms of alkenone per gram dry weight of sediment.

Chapter 5

Discussion

The Holocene cooling trend evidenced in alkenone unsaturation ratios from the northwest Atlantic is broadly consistent with other records of Holocene cooling [27, 26]. Particularly, coupled atmosphere-ocean-sea ice-vegetation model of Renssen et al. [41] demonstrated a roughly 2°C cooling of annual average temperature over the Holocene in northern North America, with the bulk of that change being accounted for by the spring and summer months.

Here we compare our records of alkenone temperature with previous records of the same parameter from the Virginia Slope, Laurentian Fan, and Emerald Basin. The general pattern of Holocene cooling, with a greater cooling magnitude farther north, is consistent between our data and previous records from the region. Possible reasons for differences in timing and magnitude of the cooling between sites are enumerated below.

We additionally compare our data with other proxies from the same region, and discuss reasons for differences between proxies. Comparisons between alkenone records and other common proxies for sea surface temperature often show somewhat different records over the Holocene [27, 21], and the evidence presented here is similar. One possible explanation for a discrepancy between proxies is variation in the production season or depth for the various species producing these proxies [27, 21]. The potential of production season to affect $U^{k'}_{37}$ at the core sites examined in this study is explored here.

Comparison between alkenone temperature records and $\delta^{18}O$ is tricky, because $\delta^{18}O$ is not a proxy affected by only temperature, as $U^{k'}_{37}$ is. The oxygen isotope content of foraminiferal shells is primarily determined by the local $\delta^{18}O$ of seawater and the local temperature, but the particular relationship between temperature and isotopic fractionation is species-dependent. Additionally, difference species and different organisms produce their shells at varying depths, so they do not purely reflect the temperature at the surface. The local $\delta^{18}O$ of seawater is influenced by many factors, including global ice volume, ocean circulation, river run-off, and local precipitation and evaporation patterns.

Foraminiferal species abundance is not affected by ice volume, ocean circulation, or precipitation-evaporation balance like $\delta^{18}O$, but species data must also be considered critically. Modern analog and transfer function data are produced by assuming that the dependence of species abundance on a variety of physical parameters has not changed with time. The idea is that certain assemblages of species that are observed together in the modern environment were also present together in ancient environments, and that the temperature they grew in was that same in those ancient environments as today. Justification of this assumption is difficult.

However, organisms that are known to be highly temperature dependent can be used alone as an indicator of temperature. The species *N. pachyderma (s.)*, the left-coiling species of *N. pachyderma*, for example, only tolerates cold environments. Its presence is used to indicate cold temperatures. The presence of *N. pachyderma (s.)* as a proxy for low temperature is more reliable than multi-species proxies, because the assumption that this particular species currently grows in the same temperature range as it did thousands of years ago is easier to accept than the assumption that many species grew in the same combination of several parameters that they did thousands of years ago.

If we assume that the alkenone temperature records presented here reflect a true change in mean annual sea surface temperatures, then we must turn to oceanographic and climatological phenomena to provide physical mechanisms for such change. Variation of ocean and atmospheric circulation patterns, including surface currents in

the slope water region and atmospheric patterns over the North Atlantic, are briefly examined as possible agents of surface temperature change. Known variation of incoming solar radiation is also discussed as a mechanism of Holocene temperature change. The possibility that seasonality could account for the temperature records presented here is examined using a simple model.

5.1 Comparison with other data

5.1.1 Alkenone data from the slope water region

Figure 5-1 shows the locations of sediment cores from which an alkenone temperature record has been measured in the northwestern Atlantic, including those presented in this study and those from Sachs et al., 2006 (Severe Cooling in Northwest Atlantic Slope Waters during the Holocene, submitted.) [44].

The alkenone temperature records with reliable age models are shown together in Figure 5-2. The most striking observation is the contrast between the northerly sites, which all show a marked decrease of temperature over the Holocene, and the relatively constant temperatures of the two southern-most locations. However, even among the northern sites there are some key differences. The temperature decrease at the three northerly locations does not occur steadily throughout the entire Holocene, nor are the changes simultaneous at all sites. At the Virginia Slope, the southernmost of the three sites presented by Sachs and coworkers [44], after a brief drop of roughly 2°C around 11 k.a., the temperature remained fairly stable until the onset of a steady decline of almost 4°C at 6 k.a. At the Emerald Basin, which is on the shelf west of the Narwhal site, the temperature fluctuated within a 2 to 3°C range until 7.5 k.a., when a 7°C decline began. The Laurentian Fan record is the most monotonic of these three; temperatures there decreased by about 3 °C between approximately 12 k.a. and 8 k.a., quickly dropped by 2°C around 8 k.a. (correlated to the 8200 kyr B.P. event), and then continued to decline 4°C more between 8 k.a. and present.

Since no age model is available for the Narwhal core MD95-2031, no direct com-

parison can be made between this site and the Emerald Basin to the west and the Laurentian Fan to the south. Though the relative timings cannot be assessed, the magnitude of cooling at Narwhal is comparable to the cooling evidenced at the Laurentian Fan and greater than the cooling at the Emerald Basin. However, the shape of the Narwhal temperature record is more similar to the Emerald Basin history, in that there was a period of temperature fluctuation within a 2°C range followed by a steady cooling of at least 7°C. Without an age model for the Narwhal core, it is impossible to reject the hypothesis that these two sites experienced a very similar temperature history.

5.1.2 δ^{18}O from KNR140-51GGC, Carolina Slope

In Figure 5-3 the alkenone SST record from the Carolina Slope is plotted against δ^{18}O data measured in the same core by Keigwin and Schlegel [22]. To plot the two datasets together, the scale for δ^{18}O was chosen to represent an equivalent range of temperature according the Craig, 1965 [8] modification of the Epstein et al., 1953 [13] calibration, assuming that the oxygen isotope composition of seawater is 0‰. This assumption is roughly accurate for the late Holocene, but provides a bias toward lower temperature in the early Holocene, when global ice volume was greater and mean δ^{18}O of sea water was thus higher. Thus the lower temperatures seemingly indicated by δ^{18}O in the early Holocene may in fact merely reflect a small ice volume effect as the last of the northern hemisphere glaciers were melting away.

5.2 Correlations between $U^{k'}_{37}$ and alkenone concentration

Three of the five cores examined here (specifically KNR140-51GGC, MD95-2028, and MD95-2031) showed a statistically significant anti-correlation between $U^{k'}_{37}$ and alkenone concentration. One of the cores (MD95-2025) showed a strong positive correlation between the two alkenone parameters, and the other (KNR140-39GGC)

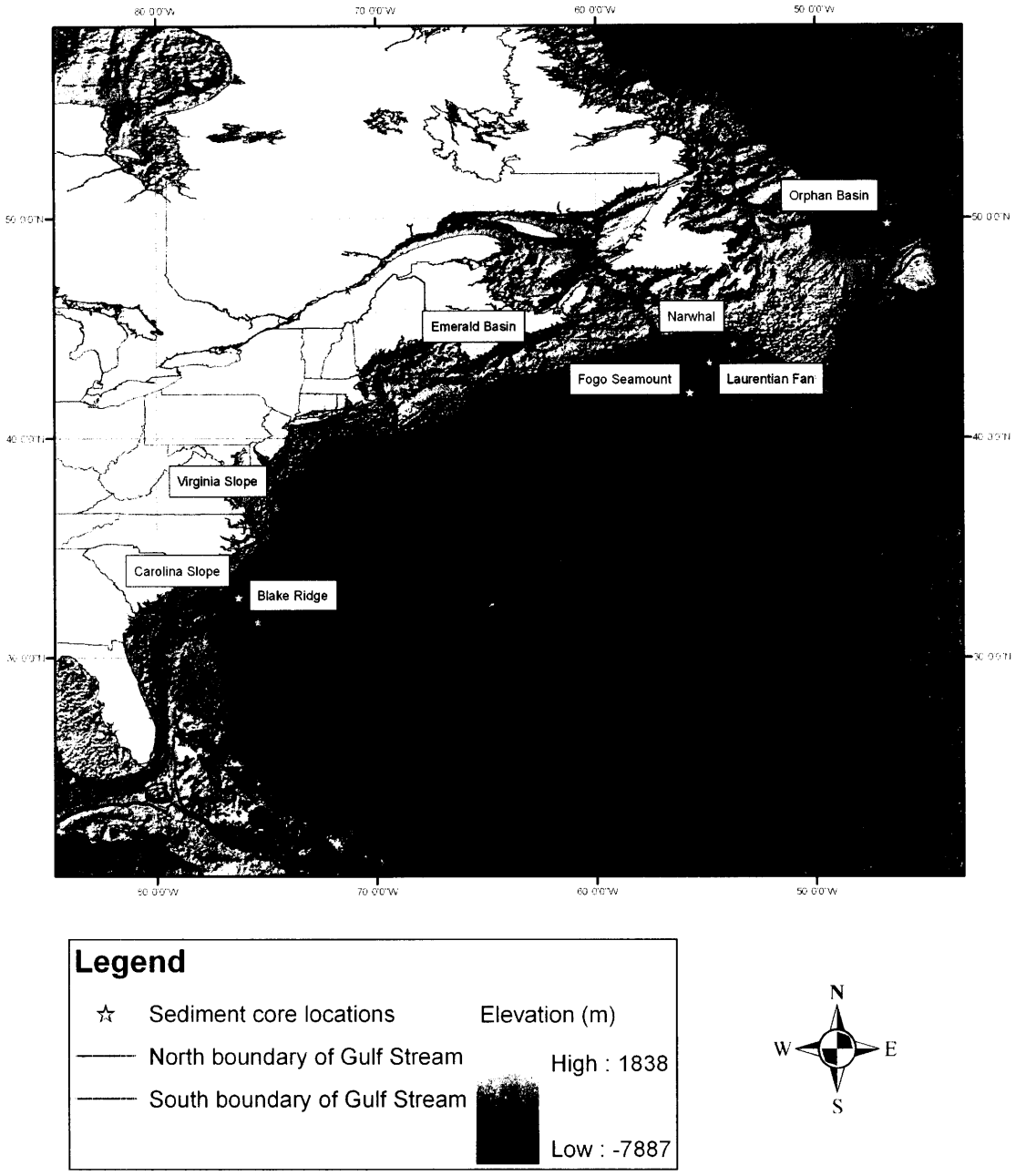

Figure 5-1: Map indicating locations of alkenone temperature data in the slope water region. Locations with green labels are from this study; pink labels indicate study sites of Sachs et al., 2006 [44].

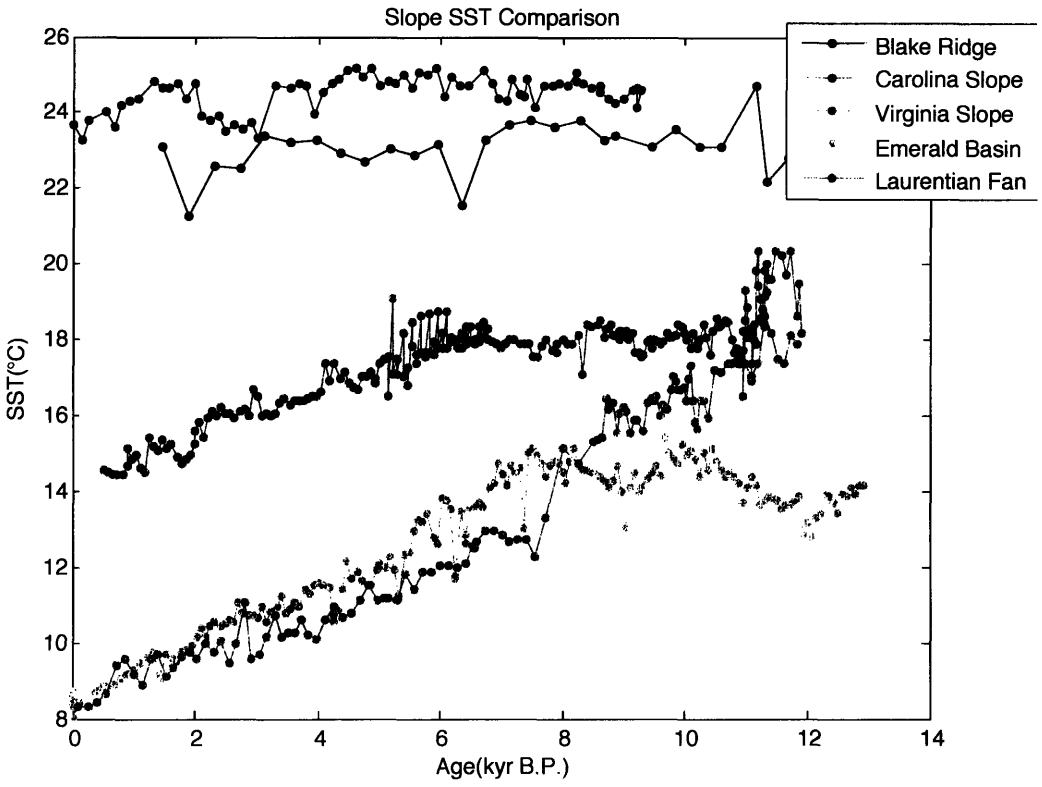

Figure 5-2: Slope water temperature data from this study and from Sachs et al., 2006 [44].

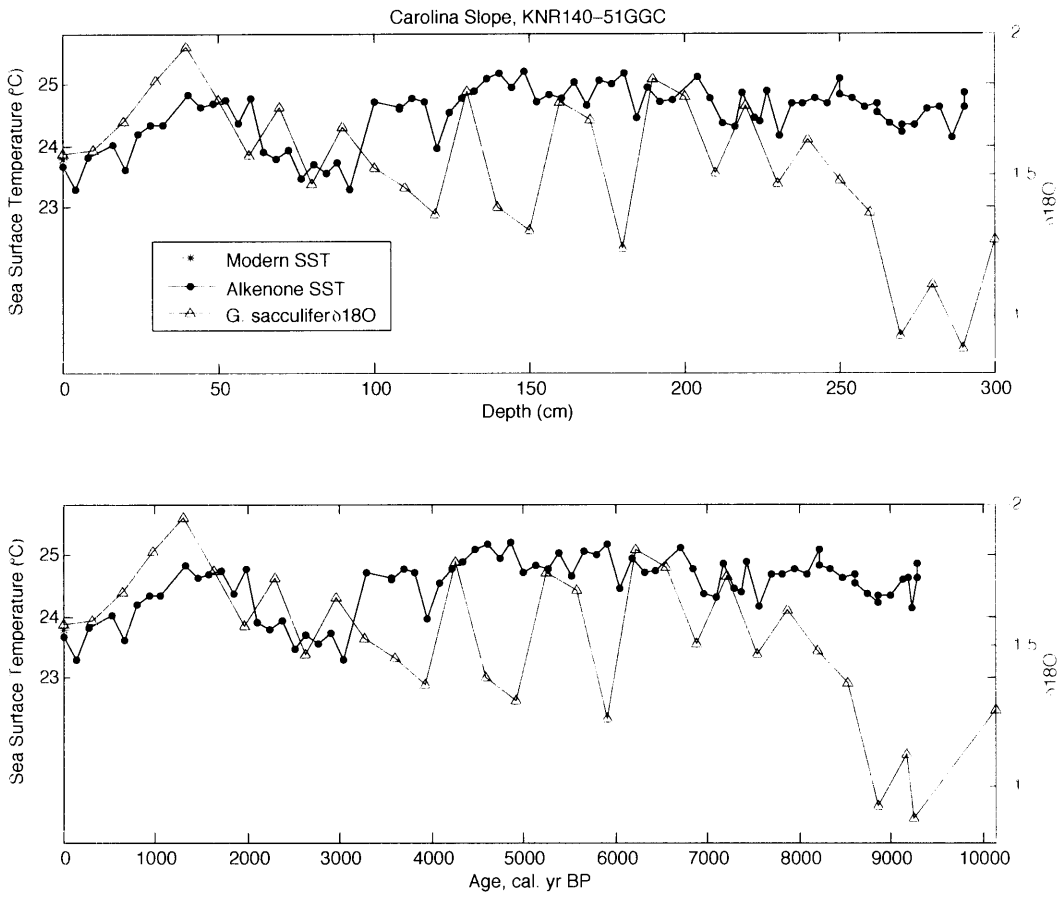

Figure 5-3: Alkenone-based sea surface temperatures (this study) and $\delta^{18}O$ measurements from G. sacculifer [23]. Scales of sea surface temperature and $\delta^{18}O$ are aligned to be equivalent according the Craig, 1965 [8] modification of the Epstein et al., 1953 [13] calibration, assuming that the oxygen isotope composition of seawater is 0‰. This assumption is roughly accurate for the late Holocene, but provides a bias toward lower temperature in the early Holocene, when global ice volume was greater and mean $\delta^{18}O$ of sea water was thus higher. The modern sea surface temperature is from the LEVITUS94 dataset [25]. The age model used in the lower panel is shown in Figure 3-2.

exhibited no significant correlation whatsoever.

Certainly, correlation does not require a causative relationship between the two. Indeed, there is a non-causative reason why an anti-correlation or correlation could exist, particularly when temperature is at either the very low or the very high end of the useful $U_{37}^{k'}$ calibration, respectively.

By definition, the parameter $U_{37}^{k'}$ is mathematically related to the total concentration of the two alkenone compounds. This can be easily seen with a reminder of the two definitions:

$$U_{37}^{k'} = \frac{C_{37:2}}{C_{37:2} + C_{37:3}} \tag{5.1}$$

and

$$\text{Concentration} = C_{37:2} + C_{37:3} \tag{5.2}$$

where $C_{37:2}$ and $C_{37:3}$ represent concentrations of the di- and tri- unsaturated alkenones, respectively.

For example, when temperatures are low and the $C_{37:3}$ compound dominates the concentration, $U_{37}^{k'}$ is also most strongly influenced by $C_{37:3}$, and the two parameters are inversely related. In this regime, as $C_{37:3}$ (and thus total concentration) increases, the apparent temperature declines as $U_{37}^{k'}$ approaches 0. At the high end of the temperature spectrum, in contrast, the total concentration is dominated by $C_{37:2}$. Thus as $C_{37:2}$ (and the total concentration) increases, $U_{37}^{k'}$ increases and approaches the asymptotic value of 1. The two parameters can therefore be expected to show positive correlation at the high end of the $U_{37}^{k'}$ temperature scale, though the alkenone temperature records here do not generally fall in the range where $U_{37}^{k'}$ becomes significantly non-linear.

An additional explanation for the statistical significance of correlation coefficients determined from these datasets comes from the definition of the correlation coefficient. Specifically, the correlation coefficient (or Pearson Product Moment Correlation) is a measure of the degree of linearity in the relationship between two parameters. When the variation of temperature is fairly small, the relationship between $U_{37}^{k'}$ and concentration of either compound is close to linear, which could lead to a stronger

(either positive or negative) correlation coefficient than if the range of $U_{37}^{k'}$ values were much larger.

This analysis provides good reason why the two parameters should show (anti-) correlation at temperature extremes, and it serves as a solid reminder that any proxy that is a ratio becomes a poor proxy as that ratio approaches either 0 or 1.

There are a few possible causative reasons why the two parameters may be related. At low temperature (and at high latitude), production of alkenones may be limited by temperature and light availability. Limitation of productivity based on temperature (or light limitation that is correlated with low temperature) would lead to a positive correlation between alkenone temperature and concentration, and it may explain why the single site that showed a positive correlation between the two parameters (MD95-2025 in the Orphan Basin) was at the highest latitude of those considered in this study. On the other hand, the core MD95-2031 shows the strongest negative correlation between $U_{37}^{k'}$ and alkenone concentration, and the difference in modern core-top temperature between MD95-2031 and MD95-2025 is only about 1.5°C. Their separation in latitude is only about 5°, so a large difference in light availability would not be expected. Additionally, the widely-used core-top calibration between $U_{37}^{k'}$ and temperature by Müller and coworkers [29] was computed through consideration of alkenone data from 60°S to 60°N, and MD95-2025 is located well within that range. Alkenone concentration in sediments is primarily affected by dilution of organic matter by terrigenous material [?]. Since much of the terrigenous material would be transported to the slope as ice rafted debris, we would expect a direct correlation between temperature and alkenone concentration, since lower temperatures would result in more ice and decreased concentration.

5.3 Impact of ocean current variability on slope water temperature

Though there is still significant debate about what dictates the mean path of the Gulf Stream, its many meanders and eddies after separation from the coast exert considerable control on the temperature and salinity properties of the slope water region [12]. The region is also influenced by a Slope Water Current that separates from the Gulf Stream, and by the colder Labrador Current which curls south along the edge of the continental shelf and around the Tail of the Banks.

The dynamics of surface current interaction in this region (and indeed the interaction between surface and deep currents) have only recently been explored, but there is some indication that these three surface currents covary. The analysis of water, heat, and salt budgets in the slope water region by Dupont and coworkers [12] indicates that in a slightly warmer climate the flux of heat from the surface ocean to atmosphere would be reduced. The result of decreased surface heat flux would be a decrease of slope water formation and a corresponding increase of Gulf Stream influence on the region. Such a mechanism could provide a way for a small amplification of overall temperature to cause a disproportionately large increase of surface temperature in the slope region.

Poor understanding of Gulf Stream separation precludes a strong implication that a radical shift in Gulf Stream separation point caused the large shift in temperature observed at the Narwhal site. However, recent studies of slope water properties and dynamics suggest that coupled interaction between surface heat flux and the Slope Water Current, Labrador Current, the Gulf Stream may make the slope region particularly sensitive to global temperature change.

5.4 Insolation and ocean temperatures

A record of Holocene insolation is shown in Figure 5-4, reproduced from Crucifix et al., 2002 [9]. This data demonstrates that northern hemisphere summer insolation

decreased over the Holocene, as did mean annual northern hemisphere insolation. Decreases in mean annual and summer insolation near the latitude of our study sites could explain the decrease in temperature evidenced by the alkenone records.

Atmospheric and particularly ocean dynamics play a strong role in moving heat around such that insolation is not the sole determinant of air and sea surface temperatures. The coupled atmosphere-ocean modeling study of Lorenz and coworkers [26] indicated that changes in insolation over the last 7000 years would be responsible for a modest mean annual warming in the slope water region. Therefore, it is unlikely that the strong cooling seen at the Narwhal site could be attributed to orbitally-forced mean annual SST change. However, their results also showed that the seasonal contrast between winter and summer temperatures in the region was lower in the middle Holocene than today. If alkenonone production occurred primarily in summer, as it is thought to in this region [19], an increase of seasonal contrast over the Holocene would manifest as an apparent warming, not cooling. This concept is explored more fully below.

5.5 Effect of seasonality on alkenone production and $U^{k'}_{37}$

Though $U^{k'}_{37}$ from marine surface sediments correlates best to mean annual sea surface temperature as opposed to seasonal average, or production-weighted seasonal temperature [29], it is nonetheless thought that the majority of alkenone export to the sediments occurs during several distinctive export events each year [36], with winter and summer export events having very different causes and $U^{k'}_{37}$ signals. Summer production produces $U^{k'}_{37}$ values that indicate a higher temperature than the mean annual SST, and winter production produces $U^{k'}_{37}$ values too low for the mean annual SST, in part because winter production and export events occur deeper in the water column than summer events. Popp et al. [34] found that alkenone production rates vary seasonally, but they were unable to determine the seasonal dependence of

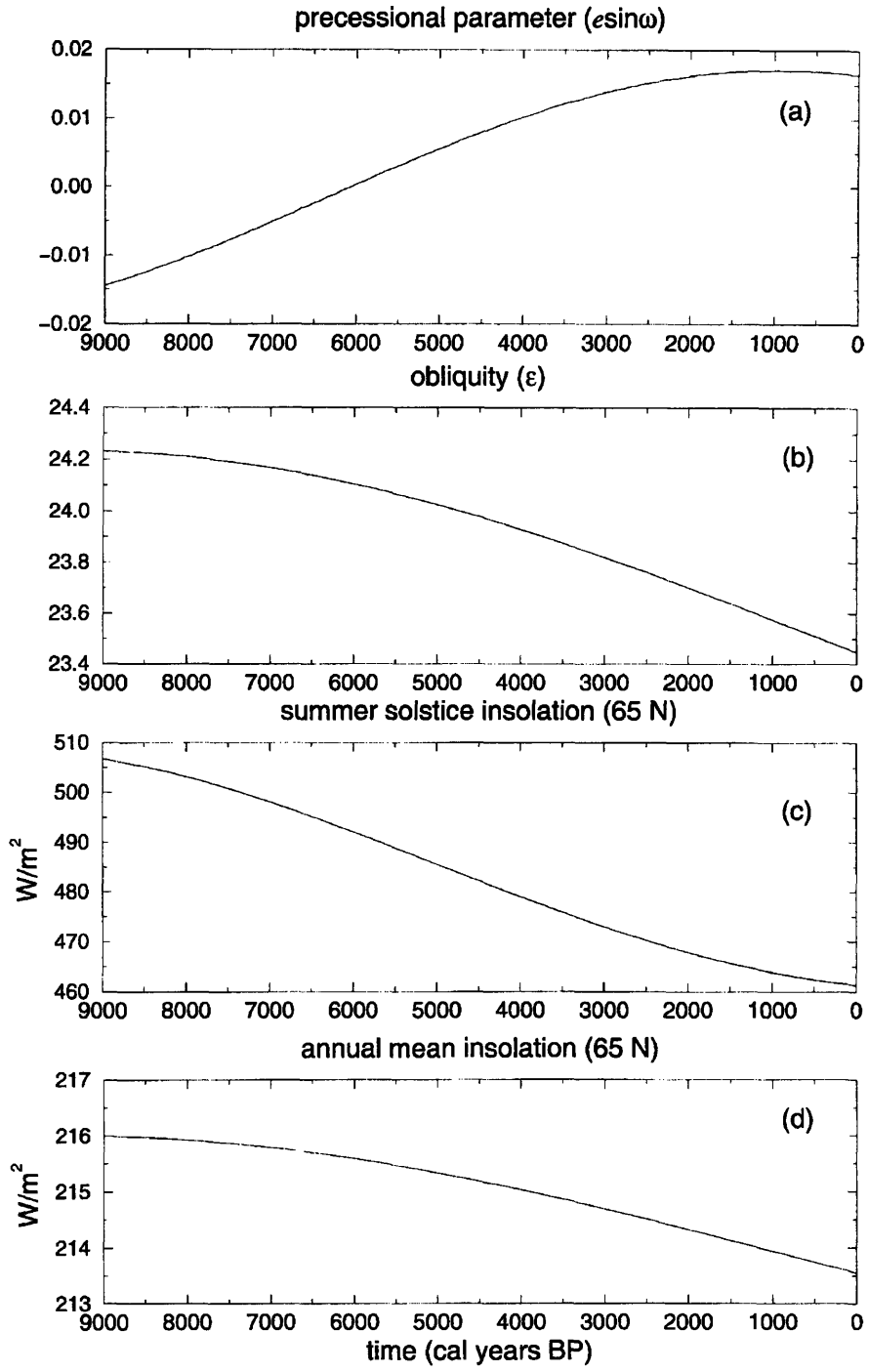

Figure 5-4: Insolation variations over the Holocene. Parameters shown are (a) Precession parameter, (b) obliquity, (c) summer solstice insolation at 65°N and (d) annual mean insolation at 65°N. From Crucifix et al., 2002 [9].

alkenone export to the sediments. They suggest that $U^{k'}_{37}$ archives should only show a disproportionate spring and summer signal if alkenone export to the sediments is increased during spring and summer.

A different picture of coccolithophorid productivity was presented by Iglesias-Rodríguez and coworkers [19]. After examining satellite data and correlating coccolithophorid blooms (mainly thought to be *E. huxleyi*) to physical parameters, they determined that blooms occur primarily in the summer when the water column becomes stably stratified, nutrient concentrations decline, and light levels are high. These observations suggest that the winter export event observed by Prahl and coworkers [36] may be a local phenomenon that is not relevant to the slope water region in the northwest Atlantic.

A spring- and summer-weighted signal seems possible, since gross biological productivity is increased in spring as nutrient-rich water upwells. The increased production could provide an increase of sinking particles that would transport alkenones from the surface mixed layer to the sediments. Alkenone-producing species make up a small proportion of the total haptophyte population [34], so during a haptophyte bloom other sinking biomass should be available to help transport the alkenone compounds out of the surface mixed layer. Even during a bloom of some other organisms (particularly diatoms), the increase of sinking biomass may help to remove alkenones present in the surface mixed layer.

Bearing in mind that production of alkenones in both summer and winter may not be realistic for our study region, we can nonetheless consider the maximum extent to which changes in the seasonality of coccolithophorid blooms could account for alkenone temperature variation by using a simple model. If production did occur in the two opposite seasons, a change in winter and summer temperatures could affect $U^{k'}_{37}$ more profoundly than the equivalent mean annual change spread evenly over the year. Additionally, a greater difference between summer and winter temperatures (greater seasonality) may change $U^{k'}_{37}$ without affecting the mean annual temperature, if production were weighted more towards one of the two seasons.

Making the broad assumption that alkenone export in the slope water region

generally can occur as either a summer or winter export event (or a combination of both), with depth characteristics similar to those observed at Station ALOHA, we can estimate the maximum range of temperature attributable to pure winter or pure summer export signals.

Core number	Location	Mean Annual SST	February SST	August SST
KNR140-39GGC	Blake Ridge	23.9°C	21.3°C	28.3°C
KNR140-51GGC	Carolina Slope	23.8°C	20.6°C	28.1°C
MD95-2028	Fogo Seamount	13.7°C	8.4°C	20.5°C
MD95-2031	Narwhal	9.2°C	2.7°C	16.6°C
MD95-2025	Orphan Basin	7.7°C	3.5°C	12.0°C

Table 5.1: Modern mean annual, February, and August sea surface temperatures at the locations of sediment cores used in this study. Data are from the LEVITUS94 database [25]. Core sites are listed in order of increasing latitude.

Modern temperature data from the LEVITUS94 database [25] is shown in Table 5.1. A comparison between mean annual, February, and August temperatures for each site demonstrates that the Fogo Seamount and Narwhal sites within the northern slope water region experience the greatest seasonal contrast in surface temperature. The two southernmost sites that are nearest the Gulf Stream show the smallest range in temperature. Orphan Basin, which is affected by the Labrador Current, shows intermediate seasonal variability.

Since the strongest temperature variability evidenced by the alkenone record comes from the Narwhal site, we can consider a simple model of alkenone production to evaluate whether changes in production season alone could explain the alkenone record at that site. We assume that there are only two possible months for a coccolithophore bloom to occur, and that export of alkenone-containing material to the sediments only occurs during these blooms. For the sake of evaluating the maximum range of $U^{k'}_{37}$ attributable to production season, and in keeping with observations of summer and winter export events [36, 34], we assume that the two export events each year occur in February and August. The $U^{k'}_{37}$ value is set by a production-weighted average of the temperature in these two months. This can be expressed as:

$$T_{alk} = 16.6 * S + 2.7 * W \tag{5.3}$$

where T_{alk} is the alkenone temperature in °C, S is the proportion of export that occurs in summer and W is the proportion of export that occurs in winter. Since we have assumed that only summer and winter export events are significant, we can further recognize that

$$W = 1 - S \tag{5.4}$$

and express the apparent alkenone temperature T_{alk} as:

$$T_{alk} = 16.6 * S + 2.7 * (1 - S) \tag{5.5}$$

and rewrite one more time to obtain:

$$T_{alk} = 13.9 * S + 2.7 \tag{5.6}$$

From these very simple assumptions, we compute that the core-top alkenone temperature of 5.8°C could be accounted for by a total alkenone export composed of 22% summer and 78% winter alkenone production and export. Similarly, the maximum alkenone temperature of 15.2° measured at 480 cm depth in the core could be explained by 90% summer export and 10% winter export of alkenones.

This analysis assumes that the modern seasonal temperature range is valid for the entire time period represented by this portion of core MD95-2031, which is difficult to justify. Note also that we have assumed that production events coincide with export events, which is not certain. Additionally, we have assumed that winter production occurs at the temperature of the ocean surface, which differs from evidence in the North Pacific that winter blooms occur in the deep chlorophyll maximum layer [36, 34]. There was no data available about winter temperatures at depth for this location. Still, in the absence of data about winter temperature profiles, Holocene seasonality, or alkenone production and export season, we still have a way to begin assessing the hypothesis that production season can account for apparent changes in alkenone-evidenced temperature.

There is no obvious reason why alkenone production should experience such a

strong shift from 90% summer to 22% summer export during the Holocene. In fact, given the satellite observations and inferred ecological niche of the coccolithophorids [19], significant production of alkenones during the winter would be surprising in the northern Atlantic.

If alkenone production remained predominantly in the summer, a decrease in seasonality over the Holocene (and implied decrease in summer maximum temperatures) would cause an apparent decrease in alkenone temperature, even if the mean annual temperature did not change.

Changes in production seasonality are unlikely to explain the entire magnitude of apparent temperature variation seen at the Narwhal site. However, either a change in alkenone production season, or a change in the summer to winter temperature contrast could explain part of the variation. Seasonality may be sufficient to explain the more modest coolings of several degrees observed in the northeast Atlantic [27].

5.6 Conclusions

Three reliable records of sea surface temperature based on alkenone unsaturation provide a sharp contrast between Holocene temperature stability on the Carolina Slope and Blake Ridge and a strong decrease in Holocene temperature in the slope water region near the Grand Banks. Alkenone evidence for a cooling at the Narwhal site is consistent with other alkenone evidence of cooling from the Emerald Basin and Laurentian Fan [44] and foraminiferal δ^{18}O and % *N. pachyderma* (s.) from the Laurentian Fan [21].

A change in seasonality of alkenone production is not likely to be sufficient to explain the temperature variation evidenced in the Narwhal record. However, the sensitivity of the slope water region to warm eddies from the Gulf Stream probably accounts for the cooling seen at Narwhal, the Emerald Basin, and Laurentian Fan. Further age constraints on the Narwhal sediment core will be necessary to compare the relative timing between these three records. A future modelling study focussed on the slope water region could help test the hypothesis that local ocean dynamics amplify

a modest Holocene cooling into the strong cooling observed here. The comparative constancy of temperature at the Carolina Slope and Blake Ridge locations is due to their proximity to the Gulf Stream.

Bibliography

[1] Jinho Ahn, Martin Whalen, Bruce L. Deck, Ed J. Brook, Paul A. Mayewski, Kendrick C. Taylor, and James W.C. White. A record of atmospheric co_2 during the last 40,000 years from the siple dome, antarctica ice core. *Journal of Geophysical Research*, 109(D13305):doi:10.1029/2003JD004415, 2004.

[2] R.B. Alley, P.A. Mayewski, T. Sowers, M. Stuiver, K.C. Taylor, and P.U. Clark. Holocene climatic instability: A prominent, widespread event 8200 yr ago. *Geology*, 25(6):483–486, June 1997.

[3] E. Bard, M. Arnold, B. Hamelin, N. Tisnerat-Laborde, and G. Cabioch. Radiocarbon calibration by means of mass spectrometric $^{230}Th/^{234}U$ and 14c ages of corals: An updated database including samples from barbados, mururoa and tahiti. *Radiocarbon*, 40:1085–1092, 1998.

[4] J. Bendle and A. Rosell-Melé. Distributions of U_{37}^{K} and $U_{37}^{K'}$ in the surface waters and sediments of the nordic seas: Implications for paleoceanography. *Geochem. Geophys. Geosyst.*, 5(Q11013):doi:10.1029/2004GC00741, 2004.

[5] Thomas Blanz, Kay-Christian Emeis, and Herbert Siegel. Controls on alkenone unsaturation ratios along the salinity gradient between the open ocean and the baltic sea. *Geochimica et Costmochimica Acta*, 69(14):3589–3600, 2005.

[6] S.C. Brassell, G. Eglinton, I.T. Marlowe, U. Pflaumann, and M. Sarnthein. Molecular stratigraphy: a new tool for climatic assessment. *Nature*, 320(6058):129–133, March 1986.

[7] Garry K.C. Clarke, David W. Leverington, James T. Teller, and Arthur S. Dyke. Paleohydraulics of the last outburst flood from glacial lake agassiz and the 8200 bp cold event. *Quaternary Science Reviews*, 23:389–407, 2004.

[8] H. Craig. Measurement of oxygen isotope paleotemperatures. In E. Tongiorgi, editor, *Stable Isotopes in Oceanography Studies of Paleotemperature*, pages 161–182. CNR Lab. Geol. Nucl., 1965.

[9] M. Crucifix, M.-F. Loutre, P. Tulkens, T. Fichefet, and A. Berger. Climate evolution during the holocene: a study with an earth system model of intermediate complexity. *Climate Dynamics*, 19:43–60, 2002.

[10] W. Dansgaard, S.J. Johnsen, H.B. Clausen, D. Dahl-Jensen, N.S. Gundestrup, C.U. Hammer, C.S. Hvidberg, J.P. Steffensen, A.E. Sveinbjörnsdottir, J. Jouzel, and G. Bond. Evidence for general instability of past climate from a 250-kyr ice-core record. *Nature*, 364(6434):218–220, 1993.

[11] J.W. de Leeuw, J.W. v.d. Meer, W.I.C. Rijpstra, and P.A. Schenck. On the occurrence and structural identification of long chain unsaturated ketones and hydrocarbons in sediments. In A.G. Douglas and J.R. Maxwell, editors, *Advances in Organic Geochemistry*, volume 12, pages 211–217, 1980.

[12] Frédéric Dupont, Charles G. Hannah, and Daniel G. Wright. Model investigation of the slope water, north of the gulf stream. *Geophysical Research Letters*, 33(L05604):doi:10.1029/2005GL025321, 2006.

[13] S. Epstein, H.A. Buchbaum, and H.A. Lowenstam. Revised carbonate-water isotopic temperature scale. *Bull. Geol. Soc. Am.*, 64:1315–1326, 1953.

[14] F.C. Fuglister and L.V. Worthington. Some results of a multiple ship survey of the gulf stream. *Tellus*, 3(1):1–14, 1951.

[15] P.M. Grootes, M. Stuiver, J.W.C. White, S. Johnsen, and J. Jouzel. Comparison of oxygen isotope records from the gisp2 and grip greenland ice cores. *Nature*, 366(6455):552–554, 1993.

[16] Morten Hald, Hanne Ebbesen, Matthias Forwick, Fred Godtliebsen, Liza Khomenko, Sergei Korsun, Lena Ringstad Olsen, and Tore O. Vorren. Holocene paleoceanography and glacial history of the west spitsbergen area, euro-arctic margin. *Quaternary Science Reviews*, 23:2075–2088, 2004.

[17] Richard N. Hiscott, Ali E. Aksu, Peta J. Mudie, and David F. Parsons. A 340,000 year record of ice rafting, palaeoclimatic fluctuations, and shelf-crossing glacial advances in the southwestern labrador sea. *Global and Planetary Change*, 28:227–240, 2001.

[18] K.A. Hughen, M.G.L. Baillie, E. Bard, A. Bayliss, J.W. Beck, C. Bertrand, C.E. Buck, G. Burr, K.B. Cutler, P.E. Damon, R.L. Edwards, R.G. Fairbanks, M. Friedrich, T.P. Guilderson, B. Kromer, F.G. McCormac, S. Manning, C. Bronk Ramsey, P.J. Reimer, R.W. Reimer, S. Remmele, J.R. Southon, M. Stuiver, S. Talamo, F.W. Taylor, J. van der Plicht, and C.E. Weyhenmeyer. Marine04 marine radiocarbon age calibration, 0-26 kyr bp. *Radiocarbon*, 46:1059–1086, 2004.

[19] M. Débora Iglesias-Rodríguez, Christopher W. Brown, Scott C. Doney, Joan Kleypas, Dorota Kolber, Zbigniew Kolber, Paul K. Hayes, and Paul G. Falkowski. Representing key phytoplankton functional groups in ocean carbon cycle models: Coccolithophorids. *Global Biogeochemical Cycles*, 16(4):doi:10.1029/2001GB001454, 2002.

[20] J. Imbrie, J.D. Hays, D.G. Martinson, A. McIntyre, A.C. Mix, J.J. Morley, N.G. Pisias, W.L. Prell, and N.J. Shackleton. The orbital theory of pleistocene climate: support from revised chronology of the marine $\delta^{18}O$ record. In A. Berger, J. Imbrie, J. Hays, G. Kukla, and B. Saltzman, editors, *Milankovitch and Climate, Part 1*, volume 126 of *NATO ASI Series C:Mathematical and physical sciences*. Reidel, Dordrecht Holland, 1984.

[21] L.D. Keigwin, J.P. Sachs, Y. Rosenthal, and E.A. Boyle. The 8200 year b.p. event in the slope water system, western subpolar north atlantic. *Paleoceanography*, 20(PA2003):doi:10.1029/2004PA001074, 2005.

[22] L.D. Keigwin and M.A. Schlegel. Ocean ventilation and sedimentation since the glacial maximum at 3 km in the western north atlantic. *Geochem. Geophys. Geosyst.*, 3(1):10.1029/2001GC000283, 2002.

[23] Lloyd D. Keigwin. Radiocarbon and stable isotope constraints on last glacial maximum and younger dryas ventilation in the western north atlantic. *Paleoceanography*, 19(PA4012):doi:10.1029/2004PA001029, 2004.

[24] T. Lee. *Variability of the Gulf Stream path observed from satellite infrared images.* PhD thesis, Graduate School of Oceanography, University of Rhode Island, 1994.

[25] S. Levitus and T. Boyer. World ocean atlas 1994 volume 4: Temperature. In *NOAA Atlas NESDIS*, volume 4. U.S. Department of Commerce, Washington, D.C., 1994.

[26] Stephan J. Lorenz, Jung-Hyun Kim, Norel Rimbu, Ralph R. Schneider, and Gerrit Lohmann. Orbitally driven insolation forcing on holocene climate trends: Evidence from alkenone data and climate modeling. *Paleoceanography*, 21(PA1002):doi:10.1029/2005PA001152, 2006.

[27] Olivier Marchal, Isabel Cacho, Thomas F. Stocker, Joan O. Grimalt, Eva Calvo, Belen Martrat, Nicholas Shackleton, Maryline Vautravers, Elsa Cortijo, Shirley van Kreveld, Carin Andersson, Nalan Koç, Mark Chapman, Laura Sbaffi, Jean-Claude Duplessy, Michael Sarnthein, Jean-Louis Turon, Josette Duprat, and Eystein Jansen. Apparent long-term cooling of the sea surface in the northeast atlantic and mediterranean during the holocene. *Quaternary Science Reviews*, 21:455–483, 2002.

[28] John Marshall, Yochanan Kushnir, David Battisti, Ping Chang, Arnaud Czaja, Robert Dickson, James Hurrell, Michael McCartney, R. Saravanan, and Martin Visbeck. North atlantic climate variability: Phenomena, impacts and mechanisms. *International Journal of Climatology*, 21:1863–1898, 2001.

[29] Peter J. Müller, Georg Kirst, Götz Ruhland, Isabel von Storch, and Antoni Rosell-Melé. Calibration of the alkenone paleotemperature index $U^{k'}_{37}$ based on core-tops from the eastern south atlantic and the global ocean (60°N-60°S). *Geochimica et Costmochimica Acta*, 62(10):1757–1772, 1998.

[30] Walter H. Munk. On the wind-driven ocean circulation. *Journal of Meteorology*, 7(2):79–93, 1950.

[31] Paul G. Myers, Augustus F. Fanning, and Andrew J. Weaver. Jebar, bottom pressure torque, and gulf stream separation. *Journal of Physical Oceanography*, 26:671–683, 1996.

[32] N. Ohkouchi, T.I. Eglinton, K.A. Hughen, E. Roosen, and L.D. Keigwin. Radiocarbon dating of alkenones from marine sediments: Iii. influence of solvent extractions procedures on c-14 measurements of foraminifera. *Radiocarbon*, 47(3):425–432, 2005.

[33] Robert S. Pickart, Theresa K. McKee, Daniel J. Torres, and Stephanie A. Harrington. Mean structure and interannual variability of the slopewater system south of newfoundland. *Journal of Physical Oceanography*, 29:2541–2558, 1999.

[34] Brain N. Popp, Fredrick G. Prahl, Richard J. Wallsgrove, and Jamie Tanimoto. Seasonal patterns of alkenone productioin in the subtropical oligotrophic north pacific. *Paleoceanography*, 21(PA1004):doi:10.1029/2005PA001165, 2006.

[35] F.G. Prahl, G.J. de Lange, M. Lyle, and M.A. Sparrow. Post-depositional stability of long-chain alkenones under contrasting redox conditions. *Nature*, 341:434–437, October 1989.

[36] F.G. Prahl, B.N. Popp, D.M. Karl, and M.A. Sparrow. Ecology and biogeochemistry of alkenone production at station aloha. *Deep-Sea Research, Part I*, 52:699–719, 2005.

[37] F.G. Prahl and S.G. Wakeham. Calibration of unsaturation patterns in long-chain ketone compositions for palaeotemperature assessment. *Nature*, 330(6146):367–369, November 1987.

[38] F.G. Prahl, G.V. Wolfe, and M.A. Sparrow. Physiological impacts on alkenone paleothermometry. *Paleoceanography*, 18(2):doi:10.1029/2002PA000803, 2003.

[39] Fredrick G. Prahl, Laurel A. Muelhausen, and Debra L. Zahnle. Further evaluation of long-chain alkenones as indicators of paleoceanographic conditions. *Geochimica et Costmochimica Acta*, 52:2303–2310, 1988.

[40] D. Raynaud, J-M Barnola, J. Chappellaz, T. Blunier, A. Indermühle, and B. Stauffer. The ice record of greenhouse gases: a view in the context of future changes. *Quaternary Science Reviews*, 19(1-5):9–17, 2000.

[41] Hans Renssen, Hugues Goosse, Thierry Fichefet, Victor Brovkin, Emmanuelle Diesschaert, and Frank Wolk. Simulating the holocene climate evolution at northern high latitudes using a coupled atmosphere-sea ice-ocean-vegetation model. *Climate Dynamics*, 24:23–43, 2005.

[42] Antoni Rosell-Melé. Interhemispheric appraisal of the value of alkenone indices as temperature and salinity proxies in high-latitude locations. *Paleoceanography*, 13(6):694–703, 1998.

[43] W.F. Ruddiman and A. McIntyre. Ice-age thermal response and climatic role of the surface atlantic ocean, 40° to 63°N. *Bulletin of the Geological Society of America*, 95:381–396, 1984.

[44] Julian P. Sachs, Carl Wunsch, John Marshall, and Lloyd D. Keigwin. Severe cooling of northwest atlantic slope waters during the holocene. submitted.

[45] E.L. Sikes, J.W. Farrington, and L.D. Keigwin. Use of the alkenone unsaturation ratio U^{k}_{37} to determine past sea surface temperatures: core-top sst calibrations and methodology considerations. *Earth and Planetary Science Letters*, 104:36–47, 1991.

[46] Elisabeth L. Sikes, John K. Volkman, Lisette G. Robertson, and Jean-Jacques Pichon. Alkenones and alkenes in surface waters and sediments of the southern ocean: Implications for paleotemperature estimation in polar regions. *Geochimica et Costmochimica Acta*, 61(7):1495–1505, 1997.

[47] H. Stommel. The westward intensification of wind-driven ocean currents. *Transactions of the American Geophysical Union*, 29:202–206, 1948.

[48] M. Stuiver, P.J. Reimer, E. Bard, J.W. Beck, G.S. Burr, K.A. Hughen, B. Kromer, G. McCormac, J. van der Plicht, and M. Spurk. Intcal98 radiocarbon age calibration 24,000 - 0 cal b.p. *Radiocarbon*, 40:1041–1083, 1998.

[49] M. Stuiver, P.J. Reimer, and R.W. Reimer. Calib 5.0 [www program and documentation], 2005.

[50] J. Dana Thompson and Jr. W.J. Schmitz. A limited-area model of the gulf stream: Design, initial experiments, and model-data intercomparison. *Journal of Physical Oceanography*, 19:791–814, 1989.

[51] Gerard J.M. Versteegh, Roel Riegman, Jan W. de Leeuw, and J.H.F. (Fred) Jansen. $U^{k'}_{37}$ values for *Isochrysis galbana* as a function of culture temperature, light intensity and nutrient concentrations. *Organic Geochemistry*, 32:785–794, 2001.

[52] J.K. Volkman, G. Eglinton, E.D.S. Corner, and J.R. Sargent. Novel unsaturated straight-chain c_{37}-c_{39} methyl and ethyl ketones in marine sediments and a coccolithophore *Emiliania huxleyi*. In A.G. Douglas and J.R. Maxwell, editors, *Advances in Organic Geochemistry*, volume 30, pages 219–227. Pergamon, Oxford, 1979.

[53] James Zachos, Mark Pagani, Lisa Sloan, Ellen Thomas, and Katharina Billups. Trends, rhythms, and aberrations in global climate 65 ma to present. *Science*, 292:686–693, April 2001.